TRIUMF

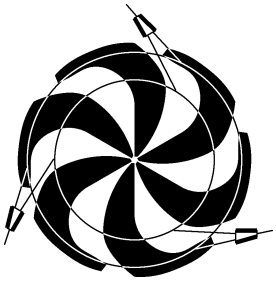

ANNUAL REPORT
SCIENTIFIC ACTIVITIES
1997

CANADA'S NATIONAL MESON FACILITY
OPERATED AS A JOINT VENTURE BY:

UNIVERSITY OF ALBERTA
SIMON FRASER UNIVERSITY
UNIVERSITY OF VICTORIA
UNIVERSITY OF BRITISH COLUMBIA

ASSOCIATE MEMBERS:

UNIVERSITY OF MANITOBA
UNIVERSITÉ DE MONTRÉAL
UNIVERSITY OF REGINA
UNIVERSITY OF TORONTO

UNDER A CONTRIBUTION FROM THE
NATIONAL RESEARCH COUNCIL OF CANADA

APRIL 1998

The contributions on individual experiments in this report are outlines intended to demonstrate the extent of scientific activity at TRIUMF during the past year. The outlines are not publications and often contain preliminary results not intended, or not yet ready, for publication. Material from these reports should not be reproduced or quoted without permission from the authors.

PARTICLE PHYSICS

Experiment 497
Measurement of the flavour conserving hadronic weak interaction

(J. Birchall, S.A. Page, W.T.H. van Oers, Manitoba)

In Expt. 497 a 221 MeV, 200 nA beam of longitudinally polarized protons is scattered from a 40 cm thick liquid hydrogen target. Figure 1 shows an overview of the experiment, including the optically pumped ion source, the cyclotron and the parity instrumentation. Approximately 4% of the incident protons scatter due to the strong nuclear force between the incident and target protons. However, because of the simultaneous presence of the weak nuclear force, the scattering fraction is expected to be enhanced very slightly, by about one part in 10^7, if the incident proton spin is aligned with the beam direction, and reduced by the same fraction if the proton spin is opposite to the beam direction. This difference is expressed as the parity violating longitudinal analyzing power, $A_z = (\sigma^+ - \sigma^-)/(\sigma^+ + \sigma^-)$, where σ^+ and σ^- are the scattering cross sections for positive and negative helicity. The goal of Expt. 497 is to measure A_z with a precision of $\pm 0.2 \times 10^{-7}$.

As illustrated in Fig. 2, the 221 MeV energy of Expt. 497 is chosen so the A_z we measure comes from the $J = 2^-$ parity mixed partial wave ($^3P_2 - ^1D_2$). This ability to select the energy is a strong advantage of the TRIUMF measurement and it simplifies the interpretation of our results. For example, if A_z is calculated using a meson exchange model with ρ and ω exchange, then the TRIUMF experiment is sensitive only to the effects of ρ exchange and can be used to extract the weak ρ-meson-nucleon-nucleon coupling constant.

Summary

- In 1997, Expt. 497 ran for four weeks in February–March, four weeks in August–September, and at the time of writing, a three-week December run is under way.

- In the February–March run Expt. 497 took 230 "data runs", corresponding to 105 hours of polarized data passing all cuts. This determined raw A_z with a statistical precision of $\pm 0.4 \times 10^{-7}$. Corrections for systematic errors also contribute an uncertainty of $\pm 0.4 \times 10^{-7}$.

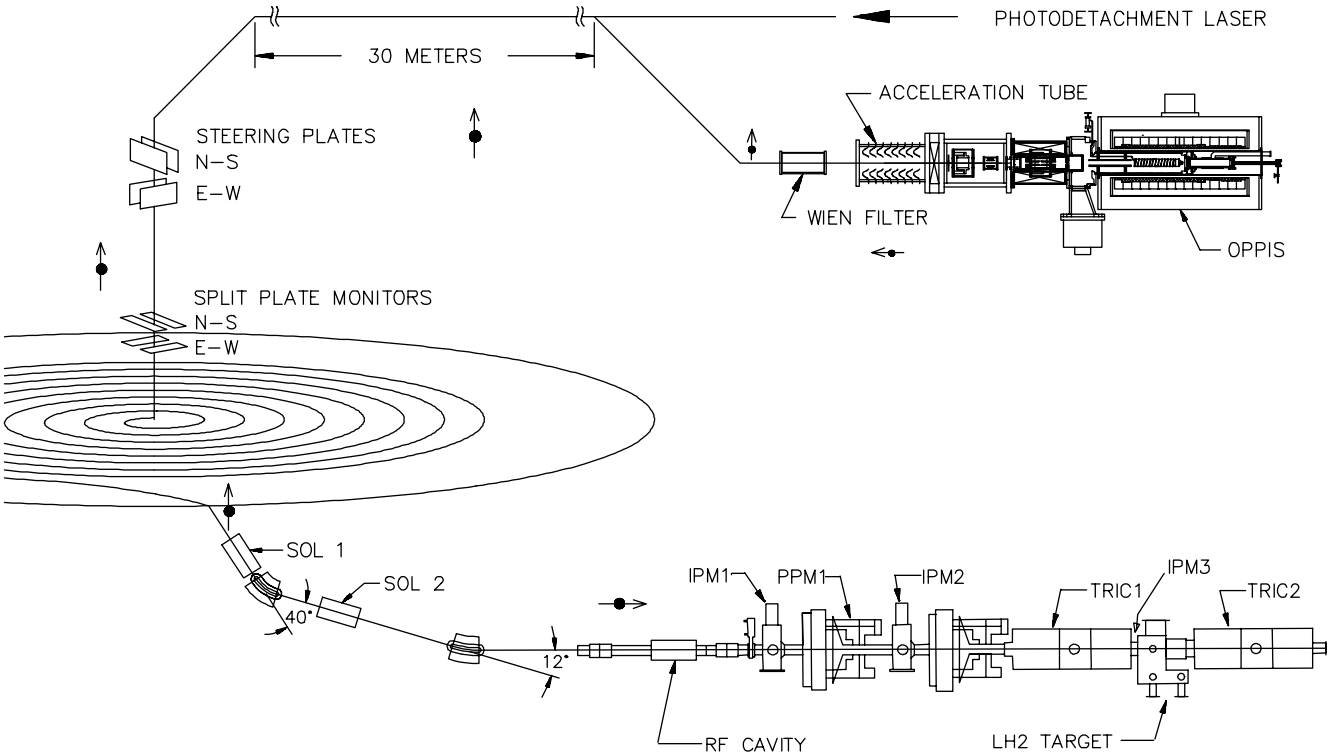

Fig. 1. General layout of the TRIUMF parity experiment. (OPPIS: optically pumped polarized ion source; SOL: spin precession solenoid; IPM: intensity profile monitor; PPM: polarization profile monitor; TRIC: transverse field ionization chamber.)

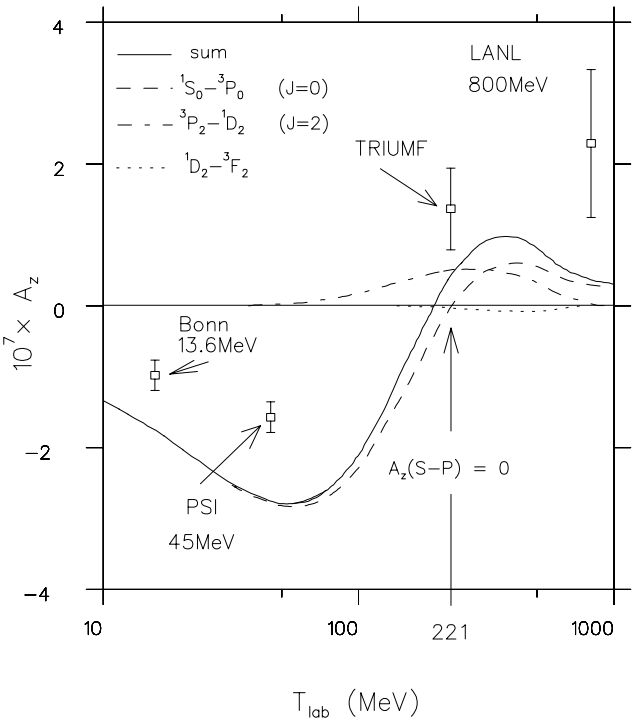

D.E. Driscoll & G.A. Miller, Phys. Rev. C40 (1989) 2159.

Fig. 2. Partial wave contributions to A_z in *pp* scattering, calculated by Driscoll and Miller, shown with existing experimental data. The TRIUMF data point is preliminary, based on the February, 1997 data set. The goal of Expt. 497 is to obtain a final error bar at 221 MeV that is comparable in size to the Bonn and PSI results.

- All measurable systematic errors are now well under control and, in fact, individual systematic corrections are generally small compared to their statistical uncertainties.
- The February data showed a residual systematic offset which had to be cancelled by averaging over runs in which the beam line helicity is reversed relative to the ion source. By changing the Wien filter polarity, it was determined that this systematic offset depended on the direction of the spin in the cyclotron.
- The August–September run was made with a special ultra-thin, 200 μg/cm^2 stripping foil. Due to technical difficulties with the liquid hydrogen target, only a week of data could be taken during the August–September run. Nevertheless, it appears that the systematic offset was not present with the 200 μg/cm^2 foil.
- For the December run, extra cooling was added to the target. At the time of writing, the target is working perfectly.

Advances in 1997

- Cyclotron and I4 performance improved:
  - Better beam current control.
  - Cyclotron tune much better defined and monitored closely by operators.
  - Method developed for using an ultra-thin stripping foil. A 200 μg/cm^2 stripping foil was mounted in a special holder. The foil is 0.5 in. high and sticks out 0.325 in. horizontally from a vertical post which fastens to the normal foil holder. In use, the foil must be shadowed so that the beam does not hit the post.
  - New instrumentation at I4 has made dramatic improvements in the measurement of energy and position modulations at the ion source.
  - To preclude electronic crosstalk from NIM or TTL levels, I4 spin confirmation is now *only* by means of a faraday rotation signal encoded as a frequency.
  - First moments vary randomly and average to small values over data sets.
- Experiment 497 hardware upgraded:
  - Removal of split-plate monitors has reduced multiple scattering.
  - Extra IPM at target location for accurate position control and better control of beam convergence.
  - Optimized beam optics have reduced *sensitivity* to first moments of transverse polarization to near zero.
  - Scintillation telescope added to measure beam halo just outside the IPM acceptance.
  - Ion chambers refurbished to provide more positive contact between electrodes.
  - For the December run, the TRIUMF Cryogenic Targets group added extra cooling in the form of two CTI-1020 refrigerators. This has been very successful. With the beam on, the target now has approximately 15 W more cooling power than that required to maintain a stable target temperature of 19 K.
- Data-taking and systematic error control methods optimized:
  - Corrections for $\frac{\delta I}{I}$ made via interleaved coherent intensity modulation (CIM) data.

– Sensitivity to beam size modulation measured by a large intentional size modulation introduced by fast, ferrite-cored quadrupoles.
– Tests with large motion confirm linear dependence of false A_z on distance from neutral axis.
– Energy modulation at I4 measured twice a day.
– Data written simultaneously to tape and disk, speeding up on-line analysis.
– Beam position setpoints under computer control.

In the following sections, selected points from these summaries are examined in more detail.

Ion source improvements

Following the February–March run, dramatic improvements were made in the ability to measure coherent energy and position modulation at the ion source. The new system uses an electrostatic analyzer and a moveable multi-strip profile monitor. The polarity of the analyzer can be reversed and the profile monitor can be moved from one side to the other. This permits the effects of coherent beam position change to be separated from the effects of beam energy change. Figure 3 shows the high quality of the new instrumentation. The left hand panel shows the energy modulation in millivolts with one laser, two lasers, and with both lasers tuned up. The right-hand panel shows the position modulation for the same sequence of laser tuning. Notice the astounding precision of a few nanometers in helicity correlated motion and a fraction of a millivolt in energy.

1997 data

Figure 4 summarizes results from the February–March and August–September runs. Results from the December run are not yet available. The first 7 data sets were taken with a 6 mg/cm^2 stripping foil, set 8 used a 2.5 mg/cm^2 foil, and sets 9 and 10 used a 200 μg/cm^2 foil.

February–March data

A total of 231 runs of "real data" were taken during February and March. 80% was polarized, 10% was unpolarized and 10% was unpolarized with intentional coherent intensity modulation. 105 hours of polarized data passed all the cuts. The preliminary result for A_z obtained from the February–March data, excluding set 8 for which the thinner stripping foil was used, is $(1.4\pm0.4\pm0.4)\times10^{-7}$, where the first error comes from statistical uncertainty in the raw A_z and the second error is dominated by statistical uncertainty in measurement of the helicity correlated quantities. Since the uncertainty in the correction is also statistical, the two errors can be combined, giving $A_z = (1.4\pm0.6)\times10^{-7}$. From Fig. 3, one can see that the true A_z, obtained by averaging the results with opposite beam line helicities, is superimposed on a large dc offset which depends on the direction of the beam in the cyclotron.

The final data set in the February–March run (set 8 on Fig. 3) was taken with a thinner stripping foil. It appeared that the DC offset was reduced, but the effect could have been statistical.

August–September data

Encouraged by the apparent reduction in the dc offset noted at the end of the February–March run with a thinner stripping foil, Expt. 497 developed a method of mounting an exceptionally thin, 200 μg/cm^2 foil for the August–September run.

The August–September run was scheduled for four weeks, but the running period was plagued by

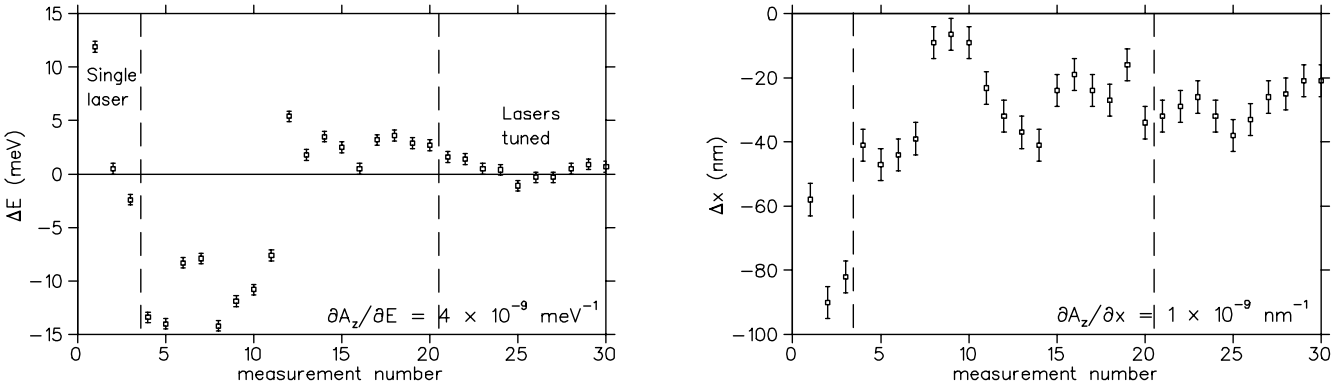

Fig. 3. Helicity correlated modulation of energy and position at the ion source. Note that the vertical scales are milli electron-volts and nanometers.

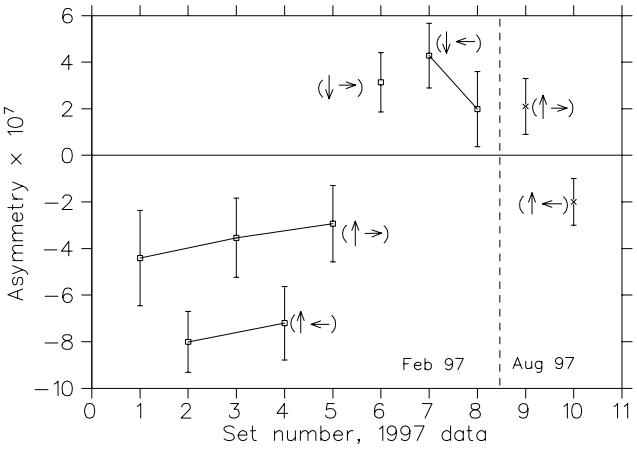

Fig. 4. Data from two of the 1997 runs after corrections for all measurable sources of systematic error. In brackets, the left-hand arrow shows the orientation of the spin in the cyclotron and the right-hand arrow shows the direction at the parity apparatus. The sign of the plotted asymmetry is such that it is equal to $+A_z$ for positive helicity at the apparatus and equal to $-A_z$ for negative helicity at the apparatus. (A right arrow indicates positive helicity.)

technical problems with the liquid hydrogen target and, in the end, only about a week of running was obtained. Nevertheless, the statistics were sufficient to suggest that the large dc offset had been eliminated. Points 9 and 10 in Fig. 3 show that the results for the two beam line helicities are now centered about zero. The off-line analysis of these data is not complete and the points are from a preliminary on-line analysis.

December run

At the time of writing, the improved liquid hydrogen target has been running perfectly with no sign of a drop in cooling power and, after a brief conditioning period, noise from the refurbished ion chambers is now as low as has been seen.

Unfortunately, the HE2 probe which was previously used to shadow the 200 μg/cm^2 stripping foil, was out of order for the December run. As an alternate, the beam line 1 extraction foil is being used. The beam removed by shadowing is extracted down beam line 1.

Corrections for systematic error

For the February–March data, total corrections for systematic error amounted to $(0.2\pm0.4)\times10^{-7}$, a value consistent with zero. The small size of the corrections is partly due to improved beam stability and quality, and partly due to a reduction in sensitivity. For example, not only did the first moments of transverse polarization average to close to zero for most data sets, but the sensitivity to first moments of transverse polarization has also been reduced by adjusting the convergence of the beam in the parity beam line so that the first moments go through zero at just the right point to reduce sensitivity to near zero. This fine tuning of the beam line was facilitated by the addition of a third intensity profile monitor inside the liquid hydrogen target vacuum enclosure.

The fact that the first moments of transverse polarization are small is very important because the sensitivity to first moment is the only sensitivity which we are not able to measure in a separate control measurement. The sensitivity to intrinsic first moments of transverse polarization must be extracted from correlations in the real data, as we have no way to "dial-in" a large artificial first moment the way we can with other beam properties.

The accuracy of corrections for coherent intensity modulation was greatly improved in 1997 by correcting on the basis of an approximately 0.1% intentional coherent intensity modulation introduced by switching off the pumping lasers and turning on the photodetachment laser for 1/10 of the data (unpolarized constitutes 1/5 of the data and the CIM laser was used in every other unpolarized state).

Although helicity correlated beam size changes are still measured in the same way with our intensity profile monitors (IPMs), corrections for these changes are now more accurate due to an improved method of measuring the sensitivity to beam size modulation. Whereas, in the past, Expt. 497 had to extract the sensitivity to beam size change from correlations in the data, in 1997 we developed a method of feeding our fast ferrite-cored steering magnets as quadrupoles and hence introducing a large artificial beam size change synchronized with the spin flip. This has improved our knowledge of the sensitivity to beam size modulation.

Future plans

At the time of writing, the December run is under way and a three week run is already scheduled for January, 1998. Beam time for the rest of the year will have to be scheduled to be compatible with ISAC commissioning, but we anticipate at least a four-week run in the summer of 1998.

Experiment 614
Precision measurement of the Michel parameters of μ^+ decay

(D.R. Gill, TRIUMF)

Precision experiments have been very important in establishing the present standard model of electroweak interactions. In the future such experiments at even higher precision will continue to be crucial, and will complement work such as that at the high energy colliders, the searches for CP violation at the B-factories, the ϕ-factory and elsewhere, rare decays at many facilities, etc. A new round of muon decay experiments, with considerable improvement over previous undertakings

is about to get under way at the meson factories, TRIUMF and PSI. The TRIUMF Expt. 614 collaboration proposes to measure with high precision the differential spectrum, $d^2\Gamma/dXd(\cos\theta)$ of positrons from the decay, $\mu^+ \to e^+\nu_e\overline{\nu}_\mu$ for polarized muons. Here X is the positron energy ($X = 1$ corresponds to the maximum positron energy $E_{\max} = 52.83$ MeV), θ is the angle between the muon spin direction and the positron momentum. The "surface" muon beam with a momentum of 29.8 MeV/c from the M13 beam line at TRIUMF will be used as the muon source.

Our experimental apparatus will consist of a superconducting solenoid, with maximum magnetic field $B = 2.2$ T collinear to the muon momentum, into which will be inserted an array of planar drift chambers (PDC's). The surface muons will be stopped inside a thin planar aluminum target (thickness 75 μm), located in the centre of the magnet. Positrons from the subsequent μ decay that go either upstream or downstream will be recorded in one of the two PDC assemblies that will be located symmetrically with respect to the stopping target. Each PDC assembly will consist of 26 planes ($13X + 13Y$) perpendicular to the magnetic field direction. The schematic arrangement of the Expt. 614 spectrometer is shown in Fig. 5.

We will measure the muon decay positron distribution, $d^2\Gamma/dXd(\cos\theta)$ in the energy range $0.4 < X \leq 1$ and in the angular range $0.5 < \cos\theta < 0.985$ with a single setting of the magnetic field.

Based on an analysis of a total of 10^9 recorded events of $\mu \to e$ decays we will determine experimentally the Michel parameters ρ, $P_\mu\xi$, δ with the significantly improved accuracies shown in the following list:

Parameter	Present(10^{-5})	Expt.614(10^{-5})
$\sigma(\rho)$	± 260	$\pm 5 \pm 13$
$\sigma(P_\mu\xi)$	$\pm 790 \pm 300$	$\pm 10 \pm 15$
$\sigma(\delta)$	$\pm 260 \pm 280$	$\pm 18 \pm 12$
$P_\mu\xi\delta/\rho$	> 0.99677 (90% C.L.)	

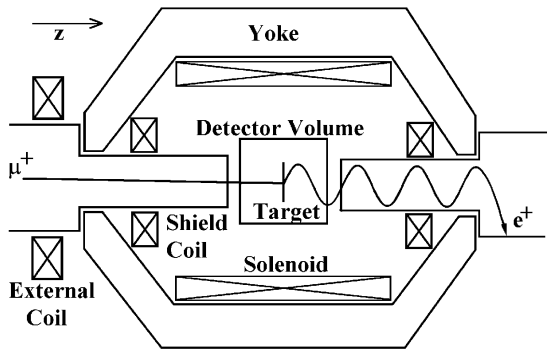

Fig. 5. Schematic layout of Expt. 614 spectrometer.

where the first error shown is statistical and the second is systematic.

The main goal of Expt. 614 is the precise testing of the $(V - A)$ structure of weak interactions in the framework of the $SU_{2L} \times U(1)$ model. It must be noted though that precise measurements of the Michel parameters will lead to strict limits on non-$(V - A)$ weak couplings. When such limits are achieved they can be used for estimates of possible violations of $(theV - A)$ model. Here we present the constraints that Expt. 614 will provide for the right-handed gauge boson (W_2) mass, the left-right mixing angle ζ and for several right-handed couplings. The precision of the Michel parameters listed above lead to the following improvments in the non-$(V - A)$ constraints:

Present	Expt. 614
90%C.L.	90%C.L.
$M(W_2) > 406\,\text{GeV}$	$M(W_2) > 820\,\text{GeV}$
$-0.056 < \zeta < 0.040$	$-0.0099 < \zeta < 0.0086$
$\lvert g^V_{RR}\rvert < 0.033$	$\lvert g^V_{RR}\rvert < 0.0161$
$\lvert g^V_{LR}\rvert < 0.060$	$\lvert g^V_{LR}\rvert < 0.0126$
$\lvert g^V_{RL}\rvert < 0.110$	$\lvert g^V_{RL}\rvert < 0.0126$

The present constraints were determined in a previous experiment at TRIUMF, Expt. 185.

Future constraints on the W_2 mass expected from other laboratories are:

TEVATRON (Run II) — 990 GeV (95%C.L.)
HERA — 370 GeV (95%C.L.).

The discovery limit for $M(W_2)$ at the LHC is predicted to be $1 \div 2$ TeV, but polarized beam with a luminosity of $L = 10^5 pb^{-1}$ and with a polarization close to 100% will be required. It is important to stress here that the measurements made at the hadron colliders are complimentary to those we will make since the limits that they establish on $M(W_2)$ are dependent on assumptions regarding the right-handed CKM matrix. This means that if, for example, the TEVATRON experiments do not discover the W_2 but a signal is seen by Expt. 614 then we are learning something about CKM_R.

During 1997 several significant developments took place regarding the mounting of Expt. 614 at TRIUMF.

1) The Russian group completed the manufacture of all the glass components required for the Expt. 614 PDCs. Thus their equipment commitment to Expt. 614

will be complete when these components are shipped to TRIUMF in 1998. The basic piece of the PDCs is a very high precision circular plate glass frame of thickness $3.2(^{+0.0}_{-0.1})$ mm with an outer diameter of $600(\pm 0.5)$ mm and an inner hole of diameter $400(\pm 0.02)$ mm. The surface of these plates is flat to 0.01 mm. The distance between the nearest chamber planes is determined by very high precision $4(\pm 0.0005)$ mm thickness glass spacer rings. The low thermal expansion coefficient of these rings (3×10^{-7} inch/inch/deg. C) guarantees that this spacing will be independent of the temperature of the detector environment. The accuracy of the assembly of these high precision pieces into a high precision chamber array is achieved by putting the glass frames on a glass winding tool ring. One face of this ring has been determined to be flat to better than 0.3 μm using an interferometer (with the ring in the vertical position in order to eliminate gravitational sag). Four 340 mm long, 15 mm wide glass rulers are put on this plane in optical contact with the ring surface so that less than one Newton ring (0.3 μm) is visible between both surfaces. These rulers have 330 diamond cut grooves into which the sense and field wires are put, thus defining the distance between the wires as that between the grooves. The grooves, 13 mm long, extend from one edge to 2 mm from the other and are at 90 degrees to the latter with a tolerance of ± 30 arc seconds. They are 15 ± 5 μm wide and not less than 5 μm deep. The assembly of the PDC array using this technique will commence at TRIUMF when the Russian team arrives in March, 1998.

2) Full scale prototypes of the Expt. 614 PDCs were constructed and tested in M13 in August. The preliminary analysis of the collected data indicates that the overall performance of the PDCs was outstanding. This preliminary analysis indicates that the resolution and efficiencies of the PDCs are ≤ 100 μm and $\geq 99\%$ respectively, well within the requirements of Expt. 614.

3) We assembled a complete Monte Carlo package of the apparatus that will be employed for Expt. 614. This includes the production and decay of pions in the production target, the transport of the muons through M13 to the point where they stop and decay within the spectrometer and the tracking of the resulting positrons within the spectrometer. We compared the capabilities of GEANT with those of EGS4 and found them to be virtually identical for the simulation of positron tracks. We have employed our Monte Carlo package to examine several design options;

- Is an M13 tune that produces an approximately parallel beam of muons to be prefered over the normal focused beam? We employed GEANT to generate pions from the proton beam passing through the 1AT1 production target and to track these pions, selecting those that stopped at the target surface. We transported the muons that resulted from the decay of these pions through M13 using the REVMOC routine. The muon rays that came out of the end of M13 were then input to our GEANT model of the spectrometer. We concluded that a focused beam is preferable and that there is an optimum position for the spectrometer relative to this focus. These studies were continuing at year's end.

- Is there an optimum shape for the 1AT1 production target? Is there an ideal shape and size of the proton beam at 1AT1? The GEANT routine described above for generating surface muons at 1AT1 was employed to search for these optimums. Target shapes for which M13 can see only one face, either the face where the proton beam enters or the side face have been compared. No conclusions have yet been reached and these studies were continuing at year's end.

- Would increasing the distance between drift chamber pairs within the spectrometer significantly improve the detector energy resolution? We found that there was, on average, an improvement in the momentum resolution and an improvement in the angular resolution. These improvements are, however, offset by the increased length of the detector, creating mechanical support problems and possibly putting some of the chamber volumes in a region of significantly nonuniform magnetic field. These studies will be continued in search of an optimum.

- Will momentum and angular resolution suffer from the addition of DME buffer zones and extra mylar foils on the drift chambers? These buffer zones and foils may be required to prevent helium diffusion into active DME regions. The answer from the Monte Carlo was that the effect, while not negligible was not going to significantly influence the accuracy of our Michel parameter determinations. Tests in the laboratory, made subsequent to the Monte Carlo studies, showed that the diffusion rate of helium through the double sided aluminized mylar foils on the chambers was small enough that an easily achievable DME flow rate of 20 cc/min would be adequate to allow us to omit the buffer zones from our design considerations.

4) NSERC approved a MIG request from the Canadian members of the collaboration.

In summary, for Expt. 614 1997 was a busy and productive year.

Experiment 705
BNL Experiments 885, 813 and 836
Strange physics at BNL: Searches for the *H* particle (BNL 813 and 836); and a search for ΛΛ hypernuclei (BNL 885) using gas microstrip chambers (705)
(C.A. Davis, TRIUMF)

Experiment 813

The analysis of data for the search for the H dibaryon is well under way. This experiment is designed to look for monoenergetic neutrons from the reaction $(\Xi^-, d)_{\rm atom} \rightarrow Hn$ where the cascade has been tagged by observing the $p(K^-, K^+)\Xi^-$ reaction simultaneously and confirming that the cascade passes through and deposits a reasonable amount of energy in a silicon detector prior to stopping in the liquid deuterium. A Univ. of Manitoba graduate student (Liping Gan) has written her thesis on the calibration reaction $(\Sigma^-, p)_{\rm atom} \rightarrow \Lambda n$ using tagged Σ's from the $p(\pi^-, K^+)\Sigma^-$ reaction with the same equipment and with similar kinematics. The neutron spectrum for the calibration is presented in Fig. 6.

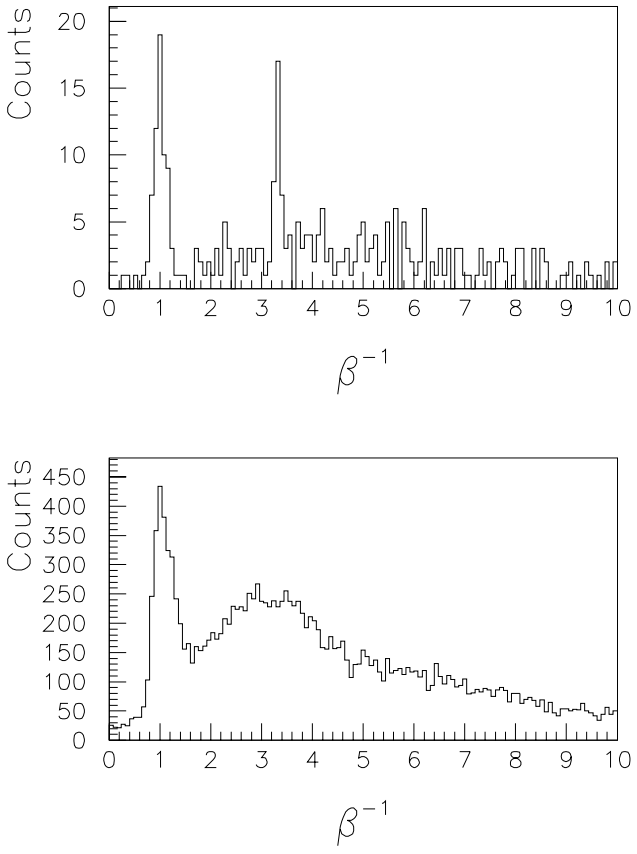

Fig. 6. Examples of neutron β^{-1} spectra for a light output threshold of 3 $\rm MeV_{ee}$ in the neutron detector. The top plot is a tagged neutron spectrum (to identify Σ's most likely to have stopped in the liquid hydrogen) and the bottom plot is an untagged neutron spectrum. The peaks at $\beta^{-1} = 1$ in both plots are the γ peaks, and the peak at $\beta^{-1} = 3.4$ in the tagged spectrum is the monoenergetic neutron signal from the $(\Sigma^-, p)_{\rm atom} \rightarrow \Lambda n$ reaction.

The clear observation of a monoenergetic neutron peak at the expected energy for Λ production clearly establishes the ability of the experimental apparatus to detect the H dibaryon for m_H within a few tens of MeV of the ΛΛ threshold. The observed number of neutrons observed in the calibration is even better than a Monte Carlo program had predicted. The H data itself is still under analysis.

Experiment 836

The results for the $^3{\rm He}(K^-, K^+)Hn$ search have now been published. No H was observed at predicted rates for the more highly bound (lower m_H) region.

Experiment 885

This experiment uses the BNL AGS D6 line to deliver a K^- beam onto a composite diamond target. Data were tagged for the double strangeness exchange reaction (K^-, K^+).

Data for the search for doubly strange hypernuclei are being analyzed by several graduate students including Michael Landry of the Univ. of Manitoba. He has recently looked for doubly strange hypernuclei through the $^{12}{\rm C}(K^-, K^+)X$ reaction by searching in the missing mass spectrum. Such a spectrum is shown in Fig. 7. Most of the large quasi-elastic peak above 11.5 $\frac{\rm GeV}{c^2}$ has been excluded. Little evidence exists for doubly strange hypernuclei in this channel. Gas microstrip chambers that were designed, built, and tested

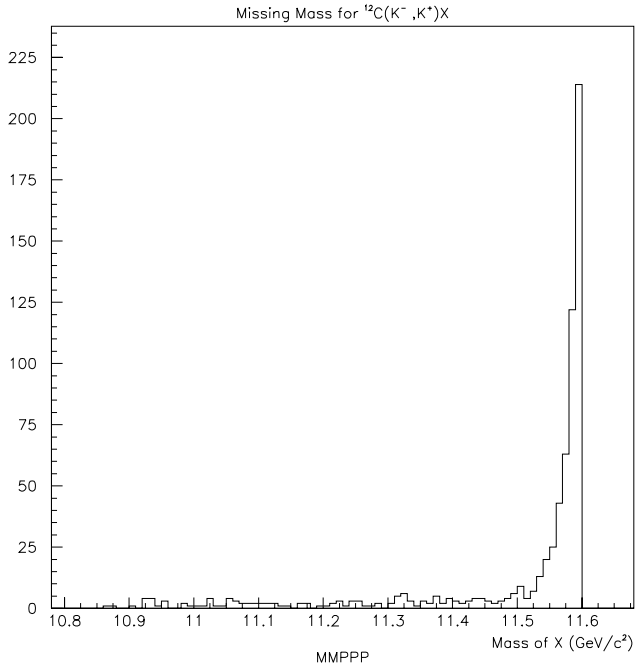

Fig. 7. Missing mass spectrum – Expt. BNL 885.

at TRIUMF (Expt. 705) were used to better define the (K^-, K^+) vertex. This information has not yet been included in the analysis, but should help clean up the missing mass spectrum.

A publication explaining our experience with the gas microstrip chambers in this experiment is in final draft form.

The ATLAS experiment on the LHC
(C.J. Oram, TRIUMF)

As described in the 1996 Annual Report, ATLAS is building a general purpose *pp* detector which is designed to exploit the full discovery potential of the Large Hadron Collider (LHC) at CERN.

The present theoretical understanding of elementary particles is in the context of the standard model. The standard model is a remarkably successful model, providing predictions which have been consistently confirmed by experiment for over two decades. Its agreement with experimental results, to enormous accuracy in some cases, makes it the most accurately verified model in science. Of the many elementary particles contained in the standard model, only the Higgs remains to be discovered. The central goal of ATLAS is the search for the Higgs particle.

There are good theoretical reasons to believe that the discovery of the Higgs will at least contain hints at, and more likely direct evidence of, what lies beyond the standard model. If the Higgs is composite, its existence requires as yet unknown ultra-strong forces. If it is elementary, it would be the only spinless particle to be discovered so far. There is a theoretical 'naturalness' problem for the masses of spinless particles. In the standard model, which is a highly nonlinear dynamical system, the elementary particles tend to take on the heaviest of all possible mass scales which in such a model are at inaccessible energies and inconsistent with other requirements of the model. All other particles discovered thus far have natural mechanisms, such as gauge and chiral symmetries, for protecting their masses so that they can lie in the observable range. For the Higgs particle, there is no such symmetry in the present model. The only theoretical scenarios which leave the Higgs particle light enough to observe are hypothetical ones, either technicolour or supersymmetry, both radical departures from the present structure of the standard model. If Higgs is seen at LHC, one of these scenarios should be seen at the same time.

Particle theory has progressed enormously over the last few decades with many appealing scenarios for physics beyond the standard model. The most likely of these is supersymmetry and the boldest of these is superstring theory. These theories are intimately related and are both radical ideas which promise a new conceptual framework for understanding elementary particles. Though far from being complete theories so far, there are superstring models which resemble the standard model in their low energy limit. These models have a great appeal as they contain a unification of fundamental forces which includes gravity. They have already had substantial impact on gravitational physics where, for example, in addition to the long sought reconciliation of gravity with quantum mechanics, they have been used to derive a fundamental understanding of black hole thermodynamics. Superstring theory is still in its infancy, but progress has been dramatic and the promise of great things to come has captured the imagination of a substantial fraction of the world's theoretical particle physicists.

The present theoretical view is that the conventional grand unification of the strong, weak and electromagnetic forces can only work in the supersymmetric extension of the standard model. In that model, the grand unified energy scale is only two decades below the Planck scale, the ultimate energy where spacetime itself has quantum fluctuations. It is not out of the realm of imagination that, at energy scales where supersymmetry would be observed, evidence for an ultimate theory of everything, at least everything that can exist once spacetime is formed, is within human grasp.

Experiments at LHC, where the ATLAS detector will take data, will probe the energy region where the Higgs particle, possibly supersymmetry, or other structures will be visible. This will be the first experimental probe of an energy region where fundamentally new physics is expected to occur in many years. There is every reason to believe that the results will be among the most dramatic ever.

Basic ATLAS design considerations

The most prominent issue for the LHC is the quest for the origin of the spontaneous symmetry-breaking mechanism in the electroweak sector of the standard model (SM). This is related to one of the most fundamental questions of physics: What is the origin of the different particle masses? New direct experimental insight is required to answer this question.

One of the possible manifestations of the spontaneous symmetry-breaking mechanism could be the existence of a SM Higgs boson (H), or of a family of Higgs particles ($H^{\pm}$, h, H and A) when considering the minimal supersymmetric extension of the standard model (MSSM). The Higgs search is therefore used as a first benchmark for the detector optimization. For the SM Higgs, the detector has to be sensitive to the following processes ($\ell = e$ or μ) in order to cover the full mass range above the expected discovery limit of LEP of about $m_H > 80$ GeV:

$H \to b\bar{b}$ from WH, ZH and $t\bar{t}H$ using a $\ell^{\pm}$ and b-tagging,
mass range $80 < m_H < 100$ GeV;

$H \to \gamma\gamma$ mass range $90 < m_H < 150$ GeV;

$H \to ZZ^* \to 4\ell^{\pm}$
mass range 130 GeV $< m_H < 2m_Z$;

$H \to ZZ \to 4\ell^{\pm}, 2l^{\pm} + 2\nu$
mass range $m_H > 2m_Z$;

$H \to WW, ZZ \to l^{\pm}\nu + 2$ jets, $2\ell^{\pm} + 2$ jets
from WW, ZZ fusion using tagging of forward jets for m_H up to about 1 TeV.

The sensitivity of ATLAS to the standard model Higgs is displayed in Fig. 8.

In addition to signatures similar to these, the MSSM Higgs searches also require sensitivity to processes such as:

$A \to \tau^+\tau^-$ $\to e\mu + \nu$'s
$\to \ell^{\pm}$ + hadrons + ν's;

$H^{\pm}$ $\to \tau^{\pm}\nu$ from $t\bar{t}$ $\to H^{\pm}W^{\mp}b\bar{b}$ and using a $\ell^{\pm}$ tag and b-tagging.
$\to$ 2jets

The observable cross sections for most of these processes are small over a large part of the mass range to be explored at the LHC. Hence it is important to operate at high luminosity, and to maximize the detectable rates above backgrounds by high-resolution measurements of electrons, photons, and muons.

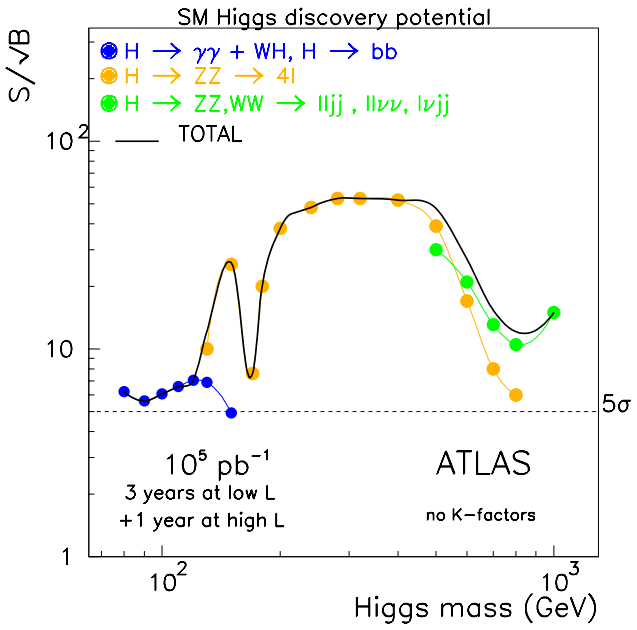

Fig. 8. Expected significance in ATLAS of the standard model Higgs boson signal, as a function of the Higgs mass, for an integrated luminosity of $10^5 \mathrm{pb}^{-1}$ for several decay channels.

Canada's participation in ATLAS

The Canadian group consists of 35 grant eligible physicists from TRIUMF, Univ. of Alberta, Carleton Univ., CRPP, UBC, Univ. of Toronto, Univ. of Victoria and York Univ. We are strongly involved in three construction projects centred around detecting hadrons in the endcap region: the hadronic endcap project, the hadronic portion of the forward calorimeter project, and the pipeline electronics for calorimetry. In addition we are committed as part of our common project contribution to providing the feedthroughs for the two endcap cryostats. TRIUMF is directly involved in all these projects and in the physics simulations. This year the group was awarded a MIG for construction of these detector elements.

The hadronic endcap project

This construction project is described in detail in the 1996 annual report. This year we have finalised the detector design and built production tooling for our first production modules. One prototype module has been finished this year and one will be finished in the first few months of 1998. The quality assurance procedures for production have been tested, and an agreement has been reached with all construction sites (Dubna, Lebedev, Protvino, MPI (Munich)) on the testing procedures. Final testing of the prototype modules starts at CERN on April 1, 1998. All construction materials have been tested for the effects of radiation damage. Also, the cold amplifiers resident on the detector have been tested for signal-to-noise, reliability, radiation resistance, and bubble creation. The amplifiers have passed these tests by the required milestone date and were passed by a production readiness review at CERN in December.

The design changes made since the 1996 engineering module are mainly minor modifications to aid in ease of construction. However, two major changes have been made. The first change provides superior protection from high voltage sparks to the cold amplifiers, resulting in a complete redesign of the method for maintaining the electric field in the liquid argon. In the old design the high voltage (2000 V) was distributed in the liquid argon gaps by copper pads connected by resistors. In the event of a spark in a liquid argon gap, a sharp voltage pulse with a peak voltage of 2000 V was seen at the input of the cold amplifier. This destroyed the input FET of that channel, along with the adjacent channels due to cross-talk from the sparked channel. The new design distributes the high voltage through a high resistive coating (of about one MΩ per square). This reduces the pulse seen at the

amplifier on the sparked channel to 2 V. Tests have shown that the amplifier can withstand in excess of 1000 such sparks without noticeable degradation. The second major modification, made as a cost saving measure, is to double the thickness of the copper plates in the rear wheel. Particles leaving the interaction region in the direction of an endcap pass through two interaction lengths of the electromagnetic endcap detector and about four interaction lengths in the front wheel of the HEC before entering the rear wheel. Hence on average a 100 GeV hadron leaves only 5% of its energy in this rear wheel. Detailed simulations of the calorimeter system showed only very minor degradation of performance by increasing the copper thickness, while major cost savings were achieved.

In March, 1998, the mechanical design will be subject to a production readiness review. This review is the final milestone that must be passed before production can start. All aspects of the design along with quality assurance procedures will be reviewed.

Study of rare *K* decays

BNL 787 (BNL-Princeton-KEK-INS(Tokyo)-Osaka-TRIUMF collaboration)

(D. Bryman, TRIUMF/Victoria)

In 1997 Brookhaven Expt. 787 reported evidence for the decay $K^+ \to \pi^+\nu\bar{\nu}$ [Adler *et al.*, Phys. Rev. Lett. **79**, 2204 (1997)]. The experiment, being carried out at the Alternating Gradient Synchrotron at Brookhaven National Laboratory, is a collaboration of TRIUMF, Univ. of Alberta, Brookhaven, Princeton Univ., KEK and Osaka Univ. The original BNL 787 spectrometer ran from 1988 to 1991 and no events were observed, allowing us to rule out branching ratios above 2.4×10^{-9}. In 1995, after the experiment was rebuilt, a new data sample was taken with a sensitivity 2.4 times greater than all prior data and a single event was discovered.

For a K^+ containing an up quark (u) and an antistrange quark ($\bar{s}$) to decay to lighter particles, the $\bar{s}$ must decay to a lighter quark. Kaons are therefore a natural laboratory for the detailed study of the weak interactions responsible for changing quark flavours. The decay $K^+ \to \pi^+\nu\bar{\nu}$ has been of interest since the 1960s when the absence of flavour changing neutral current decays was a major obstacle for the theories which grew into the present standard model. Before the mid-1970s, all known weak interactions were charged current processes even though the developing theories required a neutral current form to be as common as the charged current case. Searches in the early 1970s for other flavour changing neutral current kaon decays had found none at a rate 10^{-5} times the known charged current decays. The theory was rescued by the daring prediction of a new quark flavour whereby the flavour changing neutral currents of the new and old quarks would exactly cancel. With the discovery of the charm quark in 1974 the theory was vindicated.

Although the absence of flavour changing neutral currents in the standard model does not allow an $\bar{s}$ to change directly into a $\bar{d}$, one could imagine a higher order case where the $\bar{s}$ changes into some intermediate flavour via the charged current, and then into a $\bar{d}$ via another charged current interaction. However, while each of the three intermediate quarks – up, charm, and top – makes an allowed higher order decay, the combination of all three again cancels. But, unlike the lowest order case, this cancellation is not exact since the three intermediate quarks differ in mass; the top quark is $\sim 10^5$ times heavier than the up quark. The standard model is able to predict the small residual rate for $K^+ \to \pi^+\nu\bar{\nu}$ with a branching ratio about 1×10^{-10}.

Since a large fraction of this small rate is due to the role of the top quark, the rate is sensitive to the coupling of top to down quarks. This was recognized even before the top quark was found at Fermilab in 1994. An observed hierarchy in the weak interactions between quark generations results in the top-to-down coupling, V_{td}, being very feeble and its measurement is difficult. In fact, it is not expected to be possible to directly observe top-to-down decays at high energy accelerators in the foreseeable future. This leaves measurement of the $K^+ \to \pi^+\nu\bar{\nu}$ branching ratio as presently the most accessible way to measure V_{td}. Some other ways of determining V_{td} suffer from the fact that quarks are bound into strongly-interacting particles such as kaons and protons. Within the standard model, quantum chromodynamics (QCD) is not yet capable of precise calculations for the strong interactions of low energy quarks. In $K^+ \to \pi^+\nu\bar{\nu}$, these problems are avoided by using the measured rate of the decay $K^+ \to \pi^0 e^+ \nu$ – not a flavour changing neutral current, but having similar strong interaction effects.

The signature for $K^+ \to \pi^+\nu\overline{\nu}$ is a K^+ decay to a π^+ of momentum $P < 227$ MeV/c and no other observable product. Major background sources include the copious decays $K^+ \to \mu^+\nu$ ($K_{\mu 2}$) with a 64% branching ratio and $K^+ \to \pi^+\pi^0$ ($K_{\pi 2}$) with a 21% branching ratio. Other important background sources are beam related. The first occurs when the beam particle entering the detector is a π^+ which then scatters into the spectrometer to mimic the $K^+ \to \pi^+\nu\bar{\nu}$ signature. The second occurs when a K^+ undergoes a charge exchange reaction, becoming a long-lived neutral kaon that then decays $K_L^0 \to \pi^+\ell^-\overline{\nu}$, where ℓ is an electron or a muon. Event candidates were therefore required to have an identified K^+ stop in the target followed, after a delay of at least 2 ns, by a single charged particle track that was unaccompanied by any other decay product

or beam particle. The outgoing particle must have been identified as a π^+ with momentum (P), range (R), and kinetic energy (E) between the $K_{\pi 2}$ and $K_{\mu 2}$ peaks.

Kaons of momentum 790 MeV/c stopped in a target of plastic scintillating fibres. Measurements of the P, R and E of charged particles from the kaon decays were made using the target, a central tracking chamber, and cylindrical layers of scintillators (range stack) including two layers of tracking chambers. The momentum of a particle was measured by tracking it in the uniform 1 T magnetic field applied parallel to the beam direction. Pions were distinguished from muons by kinematics and by observing the $\pi^+ \to \mu^+ \to e^+$ decay sequence using transient digitizers in the range stack where the pions came to rest. Photons were detected in a calorimeter which completely enclosed the spectrometer, consisting of a lead/scintillator barrel detector and CsI crystal detectors covering each end. In addition, photon detectors were installed along the beam line.

An unbiased estimate of the background that would survive our analysis was a vital part of the search. To achieve the many orders of magnitude of background rejection needed, techniques were employed that incorporated redundant kinematic and particle identification measurements and efficient elimination of events with additional particles. The required rejection criteria were developed from the data without inspecting a potential signal by exploiting the redundant constraints available on each source of background to establish two independent sets of cuts. One set was inverted to enhance the background on which the rejection of the other could be measured. After correction for any correlations, the product of the rejections of the two sets of cuts for each background gave the total rejection, and hence the estimated surviving background.

In total, 0.08 ± 0.03 background events were expected in the signal region when the final analysis cuts were applied. The estimated background distribution near the signal region was tested by extending the method to predict the number of events expected to appear when the cuts were relaxed in predetermined ways and comparing with measurements from the full data, where the two sets of cuts were relaxed.

Figure 9 shows range vs. kinetic energy of the single charged track in events surviving all other cuts, including the requirement that the measured momentum be in the accepted region $211 \leq P \leq 230$ MeV/c. The rectangular box indicates the signal region with range $34 \leq R \leq 40$ cm of scintillator (corresponding to $214 \leq P_\pi \leq 231$ MeV/c for a pion) and energy $115 \leq E \leq 135$ MeV ($213 \leq P_\pi \leq 236$ MeV/c). This box encloses the upper 16.2% of the expected $K^+ \to \pi^+ \nu\bar{\nu}$ spectrum. One event was observed in the signal region. The residual events below the signal region were $K_{\pi 2}$ decays where both photons from the π^0 had been missed due to the photon detection inefficiency. A reconstruction of the candidate event is shown in Fig. 10. Since it was very unlikely for any background event to appear in the signal region, or to resemble our candidate, we conclude that we have observed a kaon decay $K^+ \to \pi^+ \nu\bar{\nu}$.

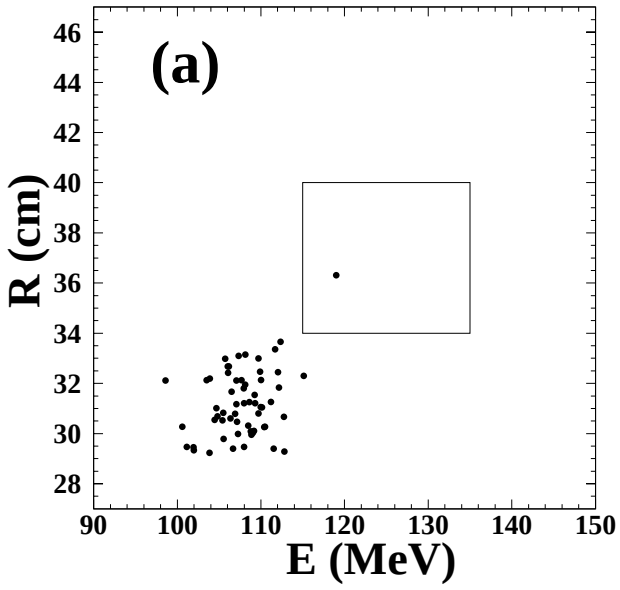

Fig. 9. Range (R) vs. kinetic energy (E) distribution for the $K^+ \to \pi^+ \nu\bar{\nu}$ data set with the final cuts applied. The box enclosing the signal region contains a single candidate event.

The acceptance calculation was verified to better than 10% by making a measurement of the $K_{\pi 2}$ branching ratio which agreed well with the accepted value. If the observed candidate event is due to $K^+ \to \pi^+ \nu\bar{\nu}$, the branching ratio is

$$B(K^+ \to \pi^+ \nu\bar{\nu}) = \frac{(\text{Number of observed candidates})/(\text{Acceptance})}{(\text{Total number of decays})} = \frac{1/0.0016}{1.49 \times 10^{12}} = 4.2^{+9.7}_{-3.5} \times 10^{-10}.$$

Based on this branching ratio, which is consistent with the standard model prediction, $|V_{td}|$ lies in the range $0.006 < |V_{td}| < 0.06$

The likelihood of the candidate event being due to a two-body decay $K^+ \to \pi^+ X^0$, where X^0 is a new massless particle that escapes detection, is small because the π^+ would have a momentum of 227.1 MeV/c, far from the observed value. Using the acceptance for $K^+ \to \pi^+ X^0$ of 0.0052 and no observed events $221 < P < 230$ MeV/c, we rule out branching ratios greater than 3.0×10^{-10}. BNL 787 has collected further

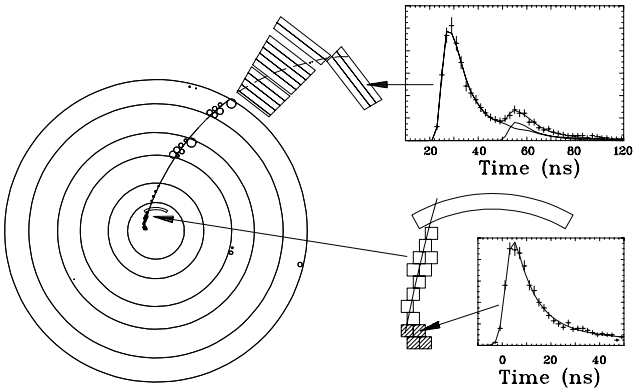

Fig. 10. Reconstruction of the candidate event. On the left is the end view of the detector. In the target and range stack, scintillators with observed energy are outlined. The large concentric circles show the layers of the tracking chamber. The small circles are signals of the passage of a charged particle. The arc is the reconstructed track, which must be tangent to the small circles. At the lower right is a blowup of the target region where the hatched boxes are kaon hits, the open boxes are pion hits, and the inner trigger counter hit is also shown. The light output sampled every 2 ns (crosses) in one of the target fibres hit by the stopping kaon is displayed along with a fit (curve) to the expected pulse shape. At the upper right of the figure is the $\pi^+ \to \mu^+$ decay signal in the range stack scintillator layer where the pion stopped. The crosses are the light output sampled every 2 ns, and the curves are fits for the first (π^+ stopping), second (μ^+ from π^+ decay), and combined pulses.

data in 1996 and 1997, and is continuing.

1997 also saw the final analysis and publication by the BNL 787 collaboration of two other rare K decays observed for the first time. Both $K^+ \to \pi^+\gamma\gamma$ [Kitching *et al.*, Phys. Rev. Lett. **79**, 4079 (1997)] and $K^+ \to \pi^+\mu^+\mu^-$ [Adler *et al.*, Phys. Rev. Lett. **79**, 4756 (1997)] have been discussed theoretically in the language of chiral perturbation theory (ChPT). In each case ChPT is able to predict the branching ratio and spectrum shape up to a single experimentally determined parameter reflecting the long-distance effects of QCD confinement which are not yet well understood at low energies.

For $K^+ \to \pi^+\ell^+\ell^-$, both the $\ell \equiv e$ and $\ell \equiv \mu$ decays are calculated in terms of w_+, which also controls the ratio of rates $\Gamma(K^+ \to \pi^+\mu^+\mu^-)/\Gamma(K^+ \to \pi^+e^+e^-)$. Various models give $0.49 < w_+ < 2.04$. Experimentally, w_+ has been evaluated from the branching ratio and spectrum shape in $K^+ \to \pi^+e^+e^-$ to be $w_+ = 0.89^{+0.24}_{-0.14}$. From this value, the branching ratio for $K^+ \to \pi^+\mu^+\mu^-$ is predicted to be $3.1^{+2.5}_{-1.2} \times 10^{-8}$. $K^+ \to \pi^+\ell^+\ell^-$ decays are also of interest for the light they can shed on the closely related decays $K_S \to \pi^0\ell^+\ell^-$, which are important in isolating the contribution of direct CP violation in the decay $K_L \to \pi^0\ell^+\ell^-$.

For this measurement the trigger selected decays in which two or three charged particles reached the range stack and none penetrated beyond 14 cm at 90°. $K^+ \to \pi^+\mu^+\mu^-$ events were sought using two experimental signatures. One required complete reconstruction of the three-track events in the drift chamber and target. The other signature used the total kinetic energy (143 MeV) of the decay obtained from the spectrometer, in which charged tracks traverse mainly the scintillator, even if one of the tracks was not reconstructed outside the target. Both signatures vetoed events with photons.

The three-track analysis yielded 13 events with an estimated background of 2.4 ± 2.2. The two-track procedure used a combined fit to signal and background in kinetic energy to yield 196.0 ± 16.7 events. The final branching ratio result obtained from combining both analyses is $5.0 \pm 0.4^{\rm stat} \pm 0.7^{\rm syst} \pm 0.6^{\rm th} \times 10^{-8}$, and implies $w_+ = 1.07 \pm 0.07$. We also find, using our result, $\Gamma(K^+ \to \pi^+\mu^+\mu^-)/\Gamma(K^+ \to \pi^+e^+e^-) = 0.167 \pm 0.036$, which is about 2σ below the ChPT prediction for a range $0.75 < w_+ < 1.13$.

The ChPT description of $K^+ \to \pi^+\gamma\gamma$ includes one undetermined coupling constant, $\hat{c}$, at $O(p^4)$ for which various models predict different values of $O(1)$ and the total branching ratio $(0.4 - 1) \times 10^{-6}$. From the measurement of the branching ratio and spectrum shape, it is possible to determine a value of $\hat{c}$ and also to examine whether next-to-leading order ($O(p^6)$) unitarity corrections which are needed to describe $K_L \to \pi^+\pi^-\pi^0$ are necessary. Observation of this decay mode in excess of the standard model rate would suggest the existence of new phenomena such as sequential decays of the form $K^+ \to \pi^+X^0, X^0 \to \gamma\gamma$, where X^0 is a massive short-lived neutral scalar particle.

To avoid background from the two-body $K_{\pi 2}$ decay with a monochromatic π^+ momentum of 205 MeV/c, we searched for the $K^+ \to \pi^+\gamma\gamma$ decay in the regions above ($P_{\pi^+} > 215$ MeV/c) and below (100 MeV/c $< P_{\pi^+} < 180$ MeV/c) the $K_{\pi 2}$ peak. Exactly two photon clusters were required in the barrel calorimeter with two-photon invariant mass not consistent with the π^0 mass as well as other kinematic constraints designed to suppress backgrounds. A total of 31 $K^+ \to \pi^+\gamma\gamma$ decay candidates survived all the cuts. The residual background was estimated by measuring the rejections of the cuts using methods similar to those used for the $K^+ \to \pi^+\nu\bar{\nu}$ analysis above. The independence of the cuts and the magnitude of the background level were confirmed by a large statistics Monte Carlo simulation. The estimated number of the total background was 5.1 ± 3.3.

The measured π^+ spectrum was compared with ChPT predictions by doing a maximum likelihood fit of $\hat{c}$ to the spectrum using the absolutely normalized

rate. The data support the inclusion of the unitarity corrections on the basis of a slightly improved $\chi^2_{\rm min}$. By assuming this spectrum shape, a total branching ratio was determined to be $(1.1\pm0.3\pm0.1)\times10^{-6}$. Our result also sets 90 % confidence upper limits, depending on X^0 mass and lifetime, on B($K^+ \to \pi^+ X^0, X^0 \to \gamma\gamma$), where X^0 is any short-lived neutral particle with a mass smaller than 100 MeV/c^2 decaying into two photons. For example, for mass 60 MeV/c^2 and lifetime $\leq 10^{-11}$ s, B$< 4 \times 10^{-8}$.

For more information see the BNL 787 Web site: http://www.triumf.ca/e787/homepage.html.

HERMES

Spin structure of the nucleon

(C.A. Miller, TRIUMF)

Deep inelastic lepton-nucleon scattering (DIS) experiments have been crucial in the development of our current understanding of the quark-gluon structure of nucleons. In the last decade, intense interest has focused on how the spins of the quarks and gluons contribute to the spin of the nucleon. Information about this spin structure can be obtained from the asymmetry measured in deep inelastic scattering of longitudinally polarized leptons from polarized nucleons with their spins parallel or anti-parallel. A series of such inclusive DIS experiments at CERN, SLAC and DESY on both proton and 'neutron' targets, recently culminating in remarkable precision, present a coherent picture. Early indications of the relatively small contribution of the quarks to the nucleon spin have been confirmed. New data from SLAC at 50 GeV and from HERMES will add to the inclusive data set as a function of Q^2, thereby improving global fits of polarized quark distribution functions. However, it is now realized that inclusive measurements are intrinsically limited in what more they can offer.

Semi-inclusive measurements involving the detection of a leading hadron in coincidence with the scattered lepton offer a means of 'flavour-tagging' to help isolate the contributions to the nucleon spin of the individual quark flavours, including the sea quarks. This is a central theme of the HERMES experiment, which is unique among polarized DIS experiments in two important respects. The targets are atomically pure nuclear-polarized H, D or ^{3}He gas in a high energy polarized electron storage ring. Hence the targets are undiluted by unpolarized nucleons in 'extraneous' materials. Also, the spectrometer detecting the scattering lepton, often in coincidence with hadron(s), combines substantial acceptance with hadron identification capability. Pion identification was included from the beginning, and kaon identification will be added for 1998. A schematic diagram of the experiment is shown in Fig. 11.

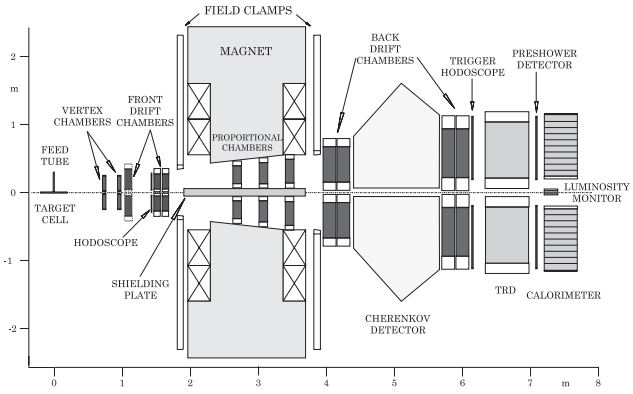

Fig. 11. Schematic side view of the HERMES spectrometer.

While data on semi-inclusive hadron production have been produced by SMC, their statistical precision is quite limited and their interpretation is complicated by model dependence related to the fact that pion identification was not possible in the SMC spectrometer. HERMES is substantially improving the precision of data on semi-inclusive processes because of the experimental advantages mentioned above. Kaon identification by the new RICH will provide flavour-tagging of strange quarks. The full database from HERMES will provide good precision on polarized quark distribution functions. In particular, the polarization related charge asymmetry in the production of pions gives information on the contribution to the nucleon spin from each flavour of valence quarks. The multiplicity of hadron h in coincidence with a DIS lepton can be written as:

$$\frac{1}{\sigma_T}\frac{dN^h}{dz} = \frac{\sum_i e_i^2 q_i(x) D_i^h(z)}{\sum_i e_i^2 q_i(x)}$$

where σ_T is the total DIS cross section, e_i is the charge of quark species i, $q_i(x)$, the quark distribution function, is the probability of finding a quark of type i with momentum fraction x, and $D_i^h(z)$, the fragmentation function, is the probability that quark i will fragment into hadron h. z is the fraction of the virtual photon energy carried by the hadron. The higher the value of z, the more probable it is that the hadron contains the struck quark. Under certain assumptions, the contribution from sea quarks cancels in the difference of the number of π^+ and π^- produced. Furthermore, the fragmentation functions cancel in ratios such as:

$$A_{\pi^+-\pi^-}(x) = \frac{(N^{\pi^+}_{\uparrow\downarrow} - N^{\pi^-}_{\uparrow\downarrow}) - (N^{\pi^+}_{\uparrow\uparrow} - N^{\pi^-}_{\uparrow\uparrow})}{(N^{\pi^+}_{\uparrow\downarrow} - N^{\pi^-}_{\uparrow\downarrow}) + (N^{\pi^+}_{\uparrow\uparrow} - N^{\pi^-}_{\uparrow\uparrow})}$$

where for example $N^{\pi^+}_{\uparrow\downarrow}$ is the number of semi-inclusive π^+ with the spins of the lepton and the target anti-parallel. This ratio can be related to valence quark spin

distributions δu_v and δd_v. For example for a proton target:

$$A_\pi^p = \frac{4\delta u_v - \delta d_v}{4u_v - d_v}.$$

Similar combinations can be written for deuterium and ^{3}He and therefore the valence spin distribution functions can be deduced. Furthermore, asymmetries in the production of $\pi^-(\bar{u}d)$ and $\mathrm{K}^-(\bar{u}s)$ have increased sensitivity to the spin contribution of light sea quarks and of strange quarks respectively. Since precise data from two targets are required to exploit the power of this technique, the definitive HERMES precision will not be available until 2000.

In summary, HERMES will give unique results on semi-inclusive processes and new structure functions (b_1, Δ, h_1), while remaining competitive for measurements of $g_1(x)$.

Canadian contribution to the experiment

Discrimination between $e^\pm$ and hadrons is provided by the combination of a transition radiation detector (TRD) and electromagnetic shower counters. The Canadian group took the responsibility for the design and construction of the TRD, and also has played a central role in the design and management of the experiment. This included the design of all the wire chambers as well as the design and commissioning of the electron polarimeter at HERA. Canadian group members were coordinators for many technical aspects of the experiment in the past and continue to provide coordinators for the following tasks: tracking chambers (A. Miller), particle identification (M. Vetterli), unpolarized physics analysis (M. Vincter), ρ-production (E. Belz). Participation in the management of the collaboration includes membership in several committees: collaboration council, planning committee, editorial board, and nominating committee.

The experiment was commisioned in the spring/summer of 1995. Data were taken in 1995 on a ^{3}He target and in 1996-97 on H. A few weeks were also spent on high luminosity running with unpolarized targets. The TRD has worked very well over the first three years of operation. The design goal was to provide a pion rejection factor of 100 at 5 GeV with a $e^\pm$ efficiency of 90% (PRF= total # of pions/hadrons divided by the # of misidentified pions/hadrons). This was achieved quasi-on-line early in the 1995 run, with typical PRF's of 120 integrated over all energies. Recent improvements to the interpretation of the TRD data using a probability based analysis have increased the PRF by a factor of up to 10. The response of a single TRD module is shown in the top panel of Fig. 12 where the particle type was determined by

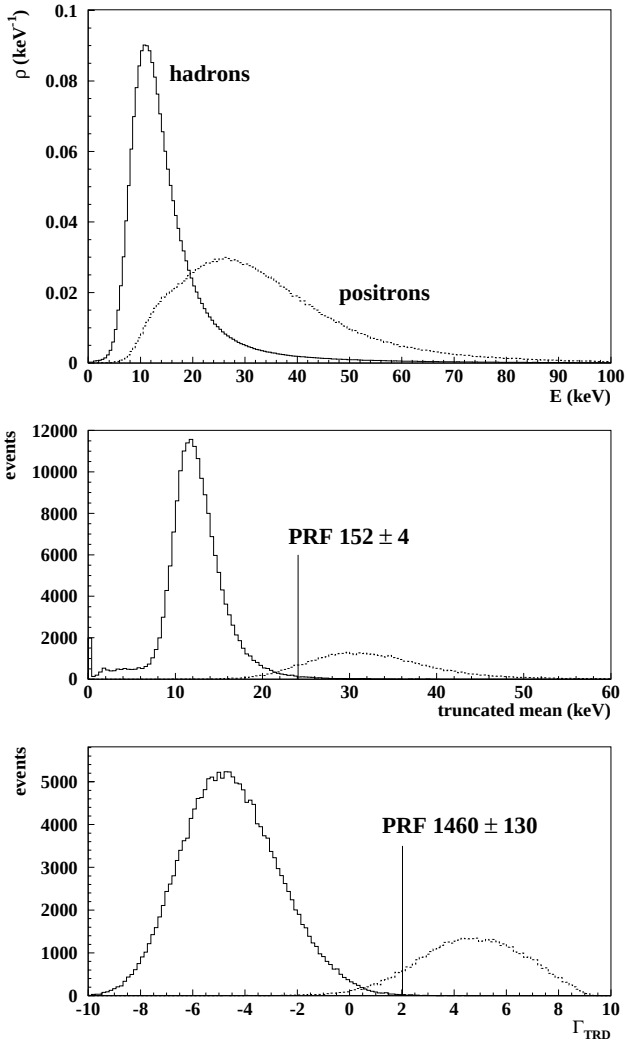

Fig. 12. TRD response for hadrons and positrons. The top panel shows the response for a single module, while the middle and bottom panels show the truncated mean and logarithmic likelihood (Γ_{TRD}) respectively. The particle type is identified for these plots using stringent cuts on the other PID detectors which provide clean samples of e^+ and hadrons. Solid lines are hadrons and dashed lines are positrons.

stringent conditions placed on the other PID detectors (calorimeter, pre-shower detector, and Čerenkov counter).

The average energy deposited by a positron is roughly twice that of a hadron due to the presence of transition radiation and the slightly higher ionization energy loss of e^+ versus hadrons. However, the long tail of the hadron distribution makes it impossible to get a good PRF with a single module. A technique used to improve the performance of TRD's is to combine the response of several modules into a "truncated mean". In the case of the HERMES TRD (6 modules), this corresponds to taking the average of the 5 modules

with the lowest energy deposit. The highest response is discarded to discriminate against events in the tail of the hadron distribution due to delta electrons from the radiator or the detector gas. The result for the truncated mean is shown in the middle panel of Fig. 12 where the improvement in the separation of the two particle types is clear. The PRF using this analysis is between 110 and 150. The PRF can be improved further by including all six modules in a probability based analysis. The response of each module is examined and a probability assigned that the signal was due to a particular particle type by comparing it to "parent distributions" of the response. The probabilities are then multiplied to obtain an overall probability for the whole TRD. Finally, the ratio of the fluxes of each particle type incident on the TRD is determined in an iterative procedure to determine a final result for the probability that a given track is of a certain particle type. The bottom panel of Fig. 12 shows the result of this analysis where the logarithmic likelihood ratio ($\Gamma_{\rm TRD}$= $\log_{10}$(Prob.(e^+)/Prob.(h^+)) is plotted. The overlap in the two distributions is now very small and leads to PRF's over 1000, much higher than the design goal. The performance of the HERMES TRD is compared to other similar detectors in Fig. 13 where the PRF is plotted versus the length of the TRD which is an indication of the number of modules. One can see that the full 6-module HERMES TRD is one of the best performing TRD's in existence.

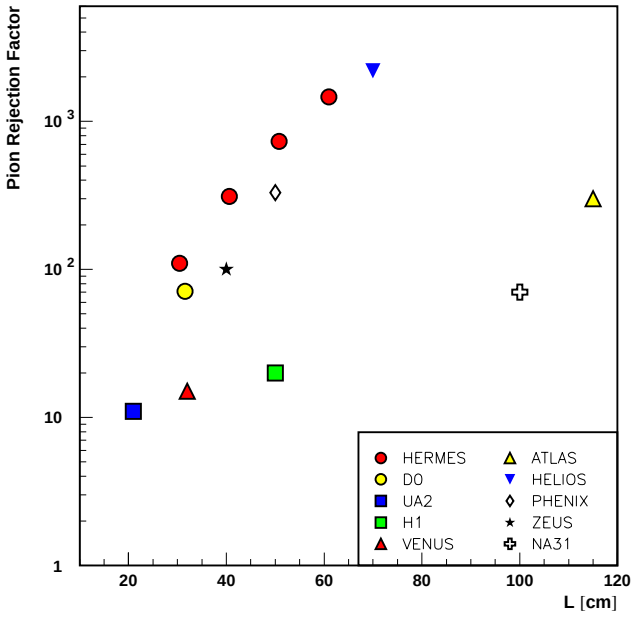

Fig. 13. Comparison of the performance of the HERMES TRD with several other similar detectors. The pion rejection factor for $\epsilon(e^+) = 90\%$ is plotted versus the length of the TRD which is a measure of the number of modules in each TRD (typically 10 cm/module).

Physics results

Inclusive scattering and spin structure functions

The spin structure function $g_1(x)$ can be determined from data on the deep inelastic scattering of longitudinally polarized leptons from polarized nucleon targets. The integral of g_1 is a measure of the contribution of the quarks to the nucleon spin. Results for $g_1^n(x)$ from the 1995 data set on ^{3}He have been published in Physics Letters [Ackerstaff *et al.*, Phys. Lett. **B404**, 383 (1997)]. However, given that 1995 was a commissioning year, the number of events collected does not represent the full data set on the neutron which will be accumulated by HERMES. A better idea of the eventual precision of the inclusive asymmetries at HERMES can be obtained by considering the preliminary results on $g_1^p(x)$ from the 1996 run on H. These data are shown in Fig. 14 where they are compared to data from SLAC-E143. The error bars are roughly equal. While HERMES has only about one third the number of bins as E143, it is of note that the full data set on the proton (1996+1997) is three times larger than shown on the graph so that the final precision of HERMES will be comparable to E143.

Semi-inclusive scattering and polarized quark distribution functions

In parallel with the inclusive measurements, HERMES has been designed to measure polarized semi-inclusive DIS. This unique data set (with identified π's and K's) will significantly improve the determination of the individual spin-dependent quark distribution functions. As is the case for inclusive scattering, one can get a good idea of the final precision of HERMES by considering the 1996 data set. Fig. 15 shows preliminary results for hadron asymmetries on the proton. The top panel is for all hadrons and also shows data from CERN (SMC). HERMES uncertainties are already competitive and will significantly improve with the inclusion of the 1997 data. The bottom panel shows data on identified pions. These data, unique to

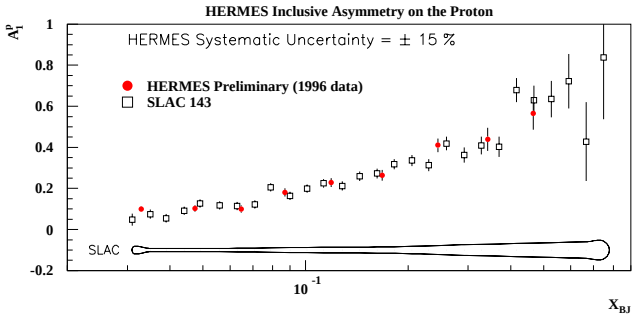

Fig. 14. Preliminary results from 1996 for the asymmetry on the proton compared to published data from SLAC-E143. Note that HERMES has collected 3 times this amount of data if the 1997 run is included.

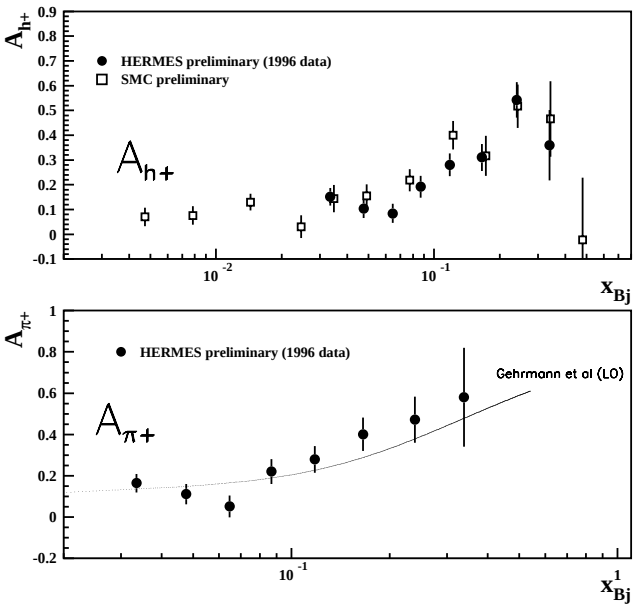

Fig. 15. Preliminary results from 1996 on the semi-inclusive hadron and pion asymmetries on the proton. Note that HERMES has collected 3 times this amount of data if the 1997 run is included.

HERMES, are sensitive to the spin of the valence quarks and can be interpreted with less model dependence than the hadron data. The extraction of δu_v, δd_v, and $\delta \bar{q}$ is under way but results are not yet ready to be shown.

Physics with unpolarized targets

Although HERMES is primarily a *polarized* deep inelastic scattering experiment, data on *unpolarized* DIS are also taken during short dedicated runs when the density of the target is increased significantly for H_2, D_2, ^{3}He, and N_2. These measurements provide good statistics on processes which do not require polarization (fragmentation functions, light quark sea asymmetry, ρ-meson production, etc.). A test of the assumption of factorization (the independence of the hard quark scattering and the subsequent hadronization of the quark) is a measurement of a known quantity such as the ratio of d-valence to u-valence quarks. This is determined from the difference in positive and negative hadrons produced on two different targets. The results from a comparison of H and D targets are plotted in Fig. 16. The HERMES results, which significantly improve on previous $e-p$ data and are of comparable precision to $\nu-p$ data, are consistent with previous experiments. Combined with the fact that d_v/u_v is independent of z, this shows that factorization holds and that HERMES data can be interpreted in the quark parton model in spite of the moderate average Q^2 of the experiment.

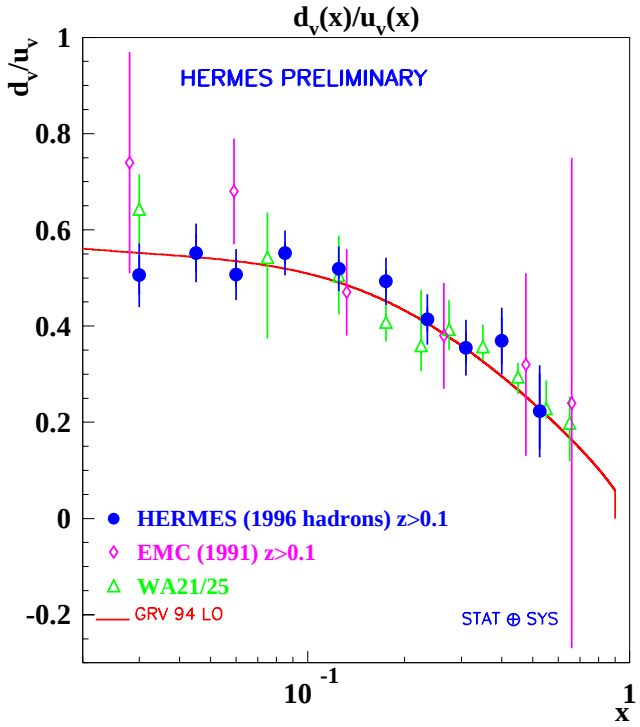

Fig. 16. Ratio of d-valence to u-valence quark distributions determined from HERMES data on unpolarized targets. The results are compared to other experiments at CERN.

Beyond providing consistency checks, the unpolarized data set can be used to determine quantities of great current interest such as the flavour asymmetry in the light quark sea. Measurements by NMC at CERN have shown that the Gottfried sum rule is violated significantly. This can be explained as an excess of $d\bar{d}$ pairs over $u\bar{u}$ pairs in the proton. HERMES unpolarized data are also sensitive to this asymmetry through a different combination of observables in hadron production than discussed in the previous example. Results for the ratio $(\bar{d}(x)-\bar{u}(x))/(u(x)-d(x))$ are shown in Fig. 17. This quantity is clearly non-zero and positive showing that there are indeed more $d\bar{d}$ pairs in the proton sea than $u\bar{u}$ pairs.

ρ meson production

Data on ρ-meson production can be used to study diffractive processes, in particular the spin characteristics of this interaction. Data with very high statistics have been taken on ^{3}He. For example, the angular distribution of the decay pions from ρ decay is shown in Fig. 18. The quantity r_{00}^{04} is a measure of the longitudinal polarization of the ρ and varies with Q^2. An analysis as a function of Q^2 is under way but it is clear already that the precision of HERMES will be very competitive with other experiments.

ρ-meson production can also be used to test the hypothesis of colour transparency. The kinematics of the scattering can be adjusted to vary the *coherence*

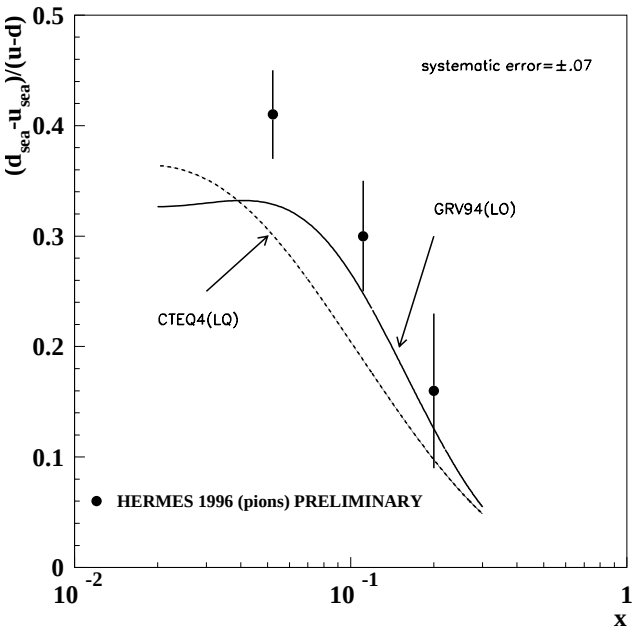

Fig. 17. Preliminary results on the asymmetry of the quark sea in the nucleon. The data are compared to a leading order calculations by Glück, Reya and Vogt and the CTEQ collaboration.

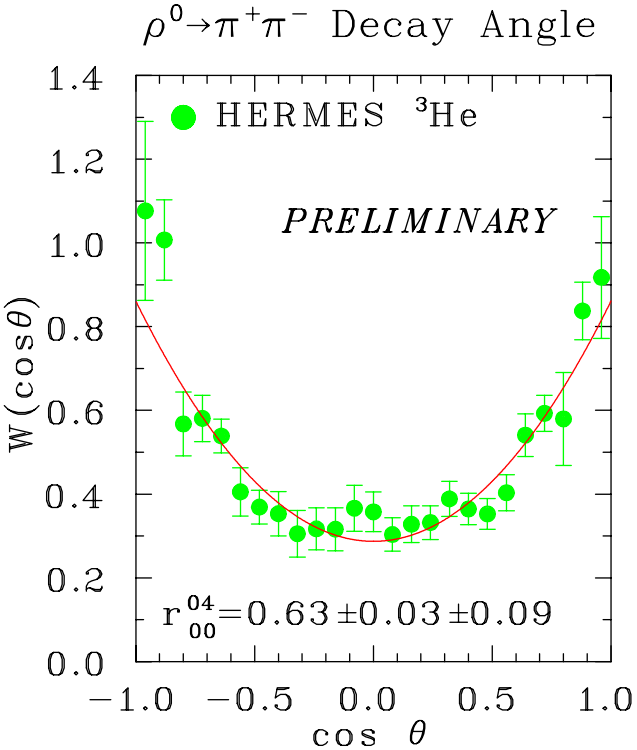

Fig. 18. Angular distribution of the π^+ from ρ decay.

length, the distance travelled by the off-shell $q\bar{q}$ pair during which it is vulnerable to hard interactions inside the nucleon, and the *expansion time* of the point-like configuration after it has been put on-shell by the Pomeron. By varying Q^2 and ν, HERMES will be able to separate these two effects and should make a definitive measurement on this long sought-after phenomenon.

Other physics

The Canadian group is involved in almost all of the analyses described in the previous section (exceptions: g_1^p, and colour transparency). There are other physics topics being addressed by the HERMES collaboration. Some of these involving members of the Canadian group are not yet ready for release, such as fragmentation functions and J/ψ production cross sections. Analyses under way at other member institutes include polarization transfer to Λ, ϕ-meson production, absolute cross sections, etc.

Outlook

The HERMES collaboration has undertaken several upgrades to the spectrometer and the targets: a muon filter wall and improved acceptance to increase our sample of J/ψ's, a *forward quadrupole spectrometer* to detect the scattered $e^{\pm}$ at very small angles and thus tag the energy of 'real' photons producing vector mesons such as the J/ψ and ϕ, upgrade of the Čerenkov detector to a RICH for kaon identification, recoil detector in the target chamber, improved rf dissociator for the atomic beam source, and development work on a laser driven H and D source. All these upgrades will result in enhanced productivity as the polarized program continues for a few more years, starting with the polarized dueterium target in 1998.

Kaonic hydrogen x-rays
KEK 228

(D.R. Gill, TRIUMF)

The $\overline{K}N$ interaction is a key issue in understanding the strong interaction in the framework of SU(3). The study of the $\overline{K}N$ interaction started in the late 1950's with bubble chamber data. These scattering data were analyzed using the K-matrix formalism of Dalitz and Tuan [Appl. Phys. **10**, 307 (1960)]. The resultant scattering lengths are largely repulsive and have a large absorption width for the isospin zero channel.

Direct measurement of the interaction scattering length can be made in a fairly model independent way through observation of the kaonic hydrogen x-rays. The kaonic hydrogen $K_\alpha(2p \to 1s)$ x-ray is shifted in energy and broadened from the pure electromagnetic value due to the $\overline{K}N$ s-wave strong interaction by

$$\Delta E(1s) + \frac{i}{2}\Gamma(1s) = 2\alpha^3\mu^2 A_{K^-p} = 412 A_{K^-p}\text{eV/fm},$$

where $\Delta E(1s) \equiv E_{\rm obs}(K_\alpha) - E_{\rm EM}(K_\alpha)$, A_{K^-p} is the K^-p scattering length, μ is the reduced mass and α is the fine structure constant. The pure electromagnetic value of the kaonic hydrogen K_α x-ray energy

($E_{\rm EM}(K_\alpha)$) includes corrections for relativistic, finite size and vacuum polarization effects. The largest uncertainty in these corrections is small, coming from the kaon mass and its charge distribution.

Measurement of the kaonic hydrogen atom x-rays began in the late 1970's. The x-ray peaks in these earlier experimental spectra were very difficult to identify and the results were inconsistent with each other, however, all agreed that the sign of the energy shift is attractive [Davies *et al.*, Phys. Lett. **83B**, 55 (1979); Izycki *et al.*, Z. Phys. **A297**, 11 (1980); Bird *et al.*, Nucl. Phys. **A404**, 482 (1983)]. An attractive shift of the atomic ground state is inconsistent with all the other data and cannot be handled in any conventional theoretical framework. This conflict became known as the kaonic hydrogen puzzle.

We completed the data-taking of KEK experiment 228 [Iwasaki *et al.*, Phys. Rev. Lett. **78**, 3067 (1997)] in 1996, completed the analysis and published the data in 1997. The result is a solution to this puzzle. Many aspects of a kaonic x-ray experiment are very difficult. For example, there is usually a huge pion contamination in the kaon beam, high resolution x-ray detectors have limited solid angles, the x-ray yield is very low and a large background is produced by $K^- p$ reactions and K^- decays in flight.

Some of the solutions taken by KEK 228 to overcome these difficulties were described in the 1995 TRIUMF Annual Report. A more detailed description of the experiment is available in Nakamura *et al.*, Nucl. Instrum. Methods [in press].

The KEK 228 experimental set-up is shown schematically in Fig. 19. The experiment was performed at the KEK 12 GeV-PS K3 beam line which was tuned to transport 600 MeV/c kaons to our target. The momentum spread, ±5%, was reduced by the wedge-shaped monochromator at the momentum dispersive point of the beam line. Kaons were selected by a single stage electrostatic separator.

Incoming beam particles were identified by the 4 layers of plastic scintillator B1 - B4. Contaminating pions were rejected by the three layers of lucite Čerenkov counters LC1 - LC3. The rejection efficiency was enhanced by time of flight (TOF) between the B1 (at K3 midplane) and B2 counters. The kaons were momentum degraded by a carbon block and stopped in the hydrogen target (100 K, 4 atm).

The two-charged-particle trigger was established by the two barrels of plastic scintillator T1 and T2.

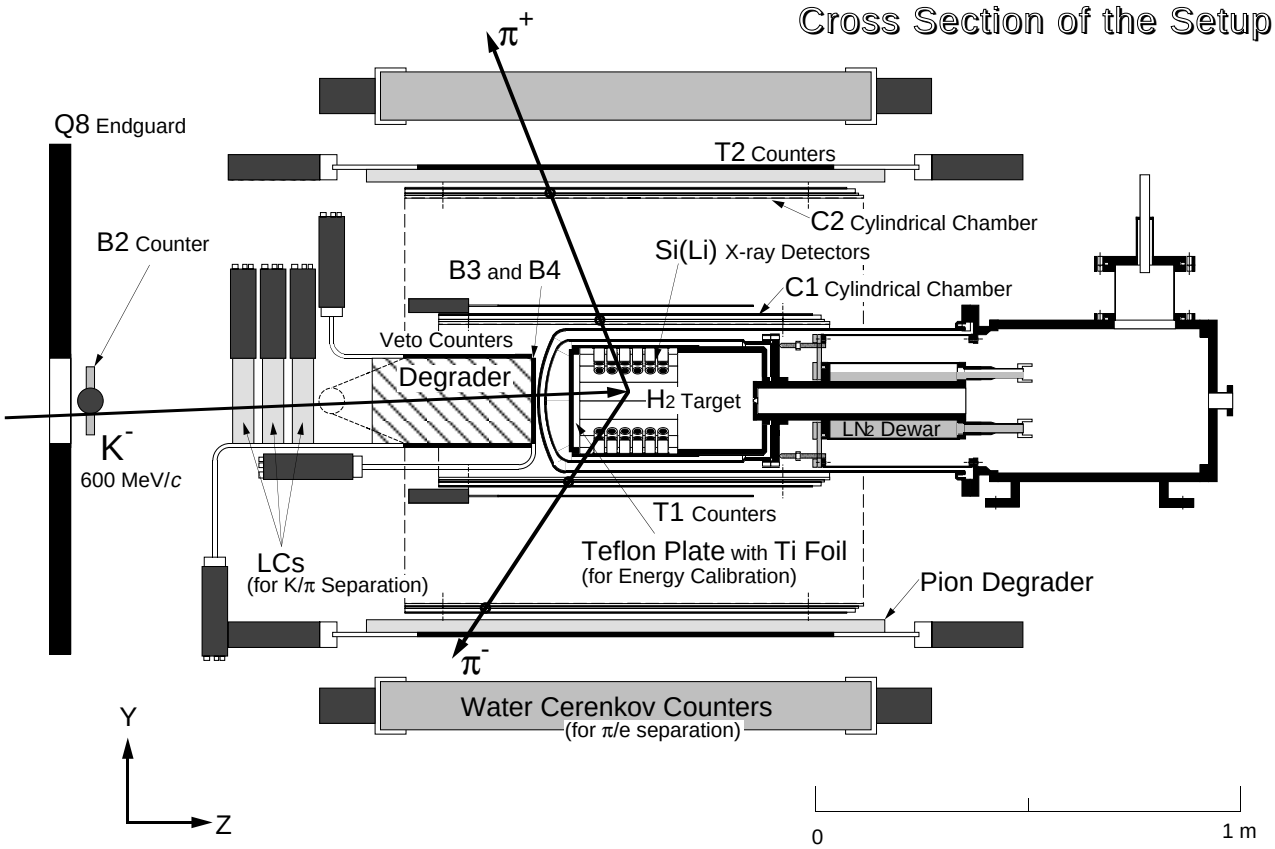

Fig. 19. The experimental set-up.

The trajectories of these particles were measured by two layers of cylindrical chambers C1 and C2.

False triggers produced by high energy γ-rays that had converted to electron-positron pairs were removed through particle identification that employed the water Čerenkov (WČ) counters.

Time-differentiated Si(Li) x-ray signals were used to determine the signal timing of each Si(Li) detector and were recorded by multi-hit TDCs. After individual detector time-walk corrections, using ADC-TDC correlations, the overall time resolution was 290 ± 10 ns (FWHM). A "prompt time" gate for kaons was defined with a width $\pm$360 ns. The x-ray energy was measured by Wilkinson type peak-sensitive ADCs using time integrated (10 μs) signals. Detector signals within the time gate were energy calibrated and then added into the summed spectrum. The overall energy resolution was found to be 407 ± 7 eV (FWHM).

After applying event selection as described above we obtained the x-ray energy spectrum shown in Fig. 20. In this spectrum, we clearly observe kaonic hydrogen K-series x-rays at about 6 and 8 keV, which are identified to be the K_α ($2p$ to $1s$) and the $K_{\rm complex}$ (from $3p$ or higher levels to $1s$), respectively. Also seen in this figure are the Ti fluorescence x-rays that are produced when K's pass through the thin titanium (Ti) foils that covered the inner surface of the target vessel. We used these Ti x-rays as an in-beam energy calibration source to monitor the gain stability. In the figure, $E_{\rm EM}(K_\alpha)$ is plotted as a dotted line. Clearly,

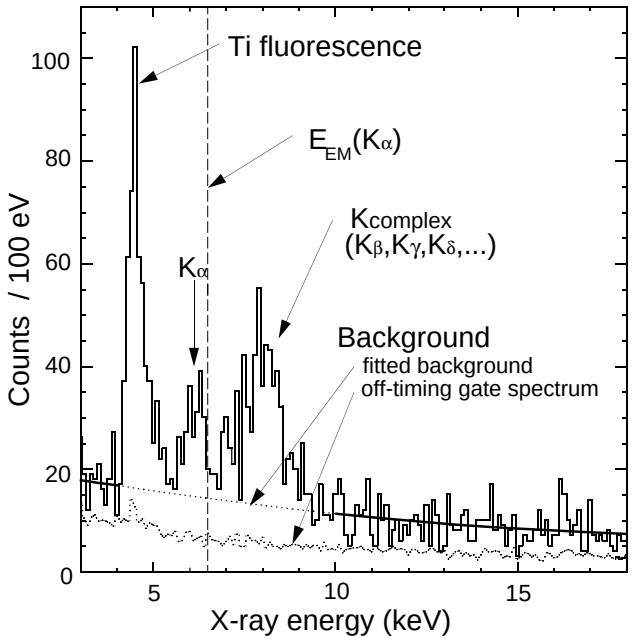

Fig. 20. Final x-ray spectrum. The dashed line is the K_α energy expected from the electromagnetic calculation. The observed K_α is on the repulsive side. Estimated accidental background is also shown.

the energy of the K_α peak is located on the lower energy side (repulsive shift) and is broadened. Because of the width of the atomic ground state ($1s$), x-rays from higher lines, overlapping each other, form a broad peak at about 8 keV.

This final x-ray spectrum shows a kaonic-hydrogen x-ray signal to background ratio drastically improved over previous experiments.

In order to avoid uncertainties due to the unknown intensity ratios of the individual K lines of the $K_{\rm complex}$, we adopted a fitting strategy that determined the energy and width primarily from the K_α. First we fitted a region around K_α peak to determine the peak position and width with a fixed background. Then, using these shift and width values to give the position and width of each complex component, the $3 \sim 10$ keV region was fit to determine the shape of $K_{\rm complex}$ and Ti fluorescence peak. We iterated this procedure, treating the tails of $K_{\rm complex}$ and Ti given by the second step as part of the background in the first step, until the energy and width converged.

The convergence was quite fast and the contribution of the $K_{\rm complex}$ tail to the K_α fit was found to be small.

We obtained an energy shift and width of K_α;

$$\Delta E(1s) = E(K_\alpha) - E_{\rm EM}(K_\alpha) = -323 \pm 63 \pm 11 \text{ eV}$$

$$\text{and } \ \Gamma(1s) = 407 \pm 208 \pm 100 \text{ eV},$$

respectively, where the first error is statistical and the second is systematic.

In our fitting procedure, discussed in the previous paragraph, the energy shift and width are determined without relying on cascade calculations. We used cascade calculations to check the peak assignment and to confirm consistency of the fitting procedure. To this end, the iterative fitting procedure of the previous paragraph was applied, using relative K-line intensities except K_α, which were generated by cascade calculations [Borie and Leon, Phys. Rev. **A21**, 1460 (1980)]. By this procedure we found a set of reasonable cascade parameter values which reproduce our data well: $\Gamma(2p) \sim 0.3$ MeV, Stark enhancement parameter $k_{\rm STK} = 1.8$ and kinetic energy of the atom $T_{\rm kin} = 1$ eV. The results confirmed that the shift and width determination of K_α is affected only weakly by the $K_{\rm complex}$ and the relative intensity of the K_α agreed to within 10%.

Simply applying Deser's formula [Deser *et al.*, Phys. Rev. **96**, 774 (1954)], we obtain the complex scattering length; $A_{K^-p} = (-0.78 \pm 0.15 \pm 0.03) + (0.49 \pm 0.25 \pm 0.12)i$ fm.

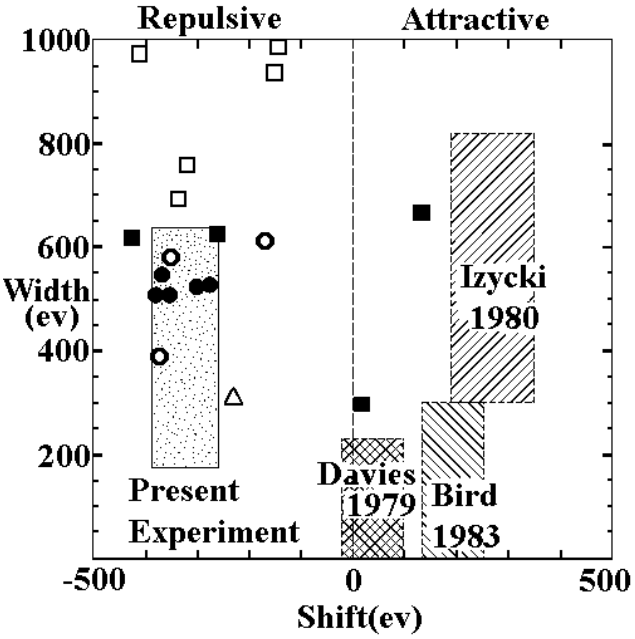

Fig. 21. Obtained shift and width of the kaonic hydrogen ground state. The statistical and systematic errors are added in quadrature. Theoretical values are also plotted.

In Fig. 21 we have plotted the one-standard-deviation region of our shift and width results in comparison with those of the previous experiments and theoretical calculations. Because the systematic error is expected to be normally distributed, we have summed the errors in quadrature. As shown in the figure, the shift given in our experiment is opposite in sign to the previous three experiments and consistent with the analysis of the low energy $\overline{K}N$ data. This resolves the long-standing kaonic hydrogen puzzle.

KEK Expt. 228 collaboration: M. Iwasaki (Tokyo Inst. of Technology), K. Bartlett, G.A. Beer, G. Mason, G. Trayling (Univ. of Victoria), D.R. Gill, L. Lee, A. Olin, M. Salomon, S. Yen (TRIUMF), R.S. Hayano, T.M. Ito, T.P. Terada (Univ. of Tokyo), S.N. Nakamura (RIKEN), H. Outa, T. Taniguchi, Y. Yamashita (KEK), R. Seki (California Inst. of Technology).

KEK Expt. 246
Search for T violation in $K_{\mu 3}$ decay (Japan-Russia-Canada-Korea-USA collaboration)
(M.D. Hasinoff, UBC; J.A. Macdonald, TRIUMF; B. Shin, Saskatchewan)

A search for transverse polarization (P_T) of muons in $K^+ \to \pi^0\mu^+\nu_\mu$ ($K^+_{\mu 3}$) decay at the $\sim 10^{-3}$ level is being carried out at the High Energy Accelerator Research Organization (KEK) in Japan by a collaboration from Canada, Japan, Korea, Russia and the USA. Such a component of the muon polarization normal to the decay plane would be an indication of the violation of time-reversal invariance. Since CPT invariance is normally assumed to be true, T violation is equivalent to CP violation. A feature of P_T in $K_{\mu 3}$ decay is that it does not have contributions from the standard model (SM) at the tree level and higher order effects are $\sim 10^{-6}$. Furthermore, since there is only one charged particle in the final state, the final state interaction, which can mimic a T violation effect, has been calculated [Zhitnitskii, Sov. J. Nucl. Phys. **31**, 529, (1980)] to be $\sim 10^{-6}$ as well. Consequently, this measurement has the potential to reveal new physics beyond the standard model.

The SM of electroweak interactions has been successful in describing all existing experimental data including the CP violation observed in neutral K decays. Nevertheless, it contains several *ad hoc* parameters and it is incomplete. Moreover, it has been suggested [Cohen *et al.*, Ann. Rev. Nucl. Sci. **43**, 27 (1993)] that the SM CP violation might not be large enough to explain the large baryonic asymmetry of the universe (BAU). Many extensions to the SM have been proposed which accommodate additional mechanisms for CP violation. Although left-right symmetric extensions do not produce a non-zero P_T from vector or axial-vector interactions, both scalar (S) and pseudoscalar (P) interactions can generate relatively large values of P_T. The three-Higgs-doublet model [Garisto and Kane, Phys. Rev. **D44**, 2038 (1991)] and the leptoquark model [Bélanger and Geng, Phys. Rev. **D44**, 2789 (1991)] can both give P_T as large as 10^{-3}. Recent SUSY model calculations [Wu and Ng, Phys. Lett. **B392**, 93 (1997)] also produce P_T as large as 2×10^{-4}. The matrix element for $K_{\mu 3}$ decay can be described [Cabbibo and Maksymowicz, Phys. Lett. **9**, 352 (1964)] by two form factors, $f_+(q^2)$ and $f_-(q^2)$. P_T is then equal to the imaginary part of the parameter $\xi = f_-(q^2)/f_+(q^2)$ multiplied by a kinematic factor.

The experiment is being carried out at the low energy kaon beam line (K5) of the KEK 12 Gev proton synchrotron (PS). The detector consists of an active scintillating fibre target which serves as a kaon stopper and vertex detector, a photon counter system which detects π^0 decay photons, a superconducting toroidal magnet spectrometer system to analyze and select μ^+s from $K^+ \to \pi^0\mu^+\nu_\mu$ decay, and 12 muon polarimeters at the quasi-focal planes of the toroidal magnet gaps. The K-decay plane is reconstructed from the μ^+ track obtained from the target, ring scintillators and wire chambers, and the π^0 direction determined from the photon detector array. The muons stop in pure aluminum plates in the polarimeter where their polarization is obtained from the distribution of decay positrons. The T violating polarization is signalled by

a net azimuthal (screw sense) asymmetry when the decay kinematics and instrumental effects are unfolded.

Our detector has sufficient kinematic coverage to simultaneously observe $K_{\mu 3}$ events with the π^0 going forward or backward along the detector (beam) axis. Such a forward/backward comparison increases our sensitivity to P_T and cancels many systematic effects to first order. Our kinematic coverage also includes a region where P_T vanishes so that a null check of our apparatus for instrumental asymmetries is possible. Moreover, the isotropic decay from stopped K^+s significantly reduces spurious effects from an asymmetric K^+ stopping distribution in the target. Finally, the e^+ polarimeters are located far from the beam axis where the normal beam associated backgrounds are low.

The principal issue in the analysis is the question of systematic effects. Notwithstanding the first order cancellations of many instrumental effects, it is important that actual instrumental asymmetries are small and understood, in order to avoid higher order subtle effects which could degrade the analyzing power by adding a bias. The data have been used to test for such effects by comparing results from the forward and backward π^0 events. These two conditions can exhibit differences due to muon stopping distributions in the polarimeter and to small rotations of the decay plane with respect to the polarimeter and magnetic fringe field. It is also necessary to determine the dependence of P_T on all the selection criteria (cuts) used in the analysis. These studies indicate that systematic errors from the forward/backward effects should be well below the $\Delta\ P_T < 10^{-3}$ level.

The data obtained so far represent about $\sim 1/3$ of our anticipated statistics. Unfortunately, the data acquired in the November-December period were limited by poor beam quality from the PS operating at a lower energy in order to avoid radiation interference with construction activity. A preliminary result based on a subset of the existing data is $P_T = -4.9 \pm 6.5 \times 10^{-3}$, with a corresponding value of the T violating parameter, Im $\xi = -0.016 \pm 0.021$, for the maximal case when Re $\xi = 0$. Further refinements to the analysis and additional running in the next two years are expected to improve the statistics-limited sensitivity to the goal of $\Delta\ P_T = 1.1 \times 10^{-3}$.

In 1997 the experimental apparatus was largely unchanged with one exception. The central cylindrical tracking drift chamber (C1) was removed after the October, 1996 run and returned to TRIUMF for modification. The inner and outer cylinders support the spiral cathode-strip foils from which axial position information is obtained. Initially the outer cylinder was constructed from very thin (0.1 mm) carbon fibre; this was replaced with a fibreglass epoxy cylinder after it was discovered that the high cathode-strip capacitance and corresponding low signal amplitudes were a result of the conductivity of the carbon fibre. The signals from the inner cathode strips were also degraded by the proximity of the inner carbon-fibre cylinder. Since this inner cylinder bears the tension load of the chamber wires the strength of carbon fibre was essential and a new cylinder was constructed with a smaller diameter which allowed the space needed to insert a 0.75 mm layer of Rohacell between the cathode foil and the carbon fibre in order to reduce the capacitance by a factor of about 13.

The new chamber was tested with sources and with beam in M13 before being shipped back to KEK in September. Excellent cathode signals were obtained with a significantly reduced noise level. After installation in the detector at KEK, cosmic-ray tests were conducted to determine the C1 position resolution. These data and those obtained in the November-December run are currently undergoing analysis.

TJNAF Experiment 91-017
Measurement of the flavour singlet form factors of the proton
(W.T.H. van Oers, Manitoba)

The structure of the nucleon at low energies in terms of the quark and gluon degrees of freedom is not well understood. The $G0$ experiment is to measure two proton ground state matrix elements which are sensitive to point-like "strange" quarks and hence to the quark-antiquark sea in the proton. The matrix elements of interest are the elastic scattering vector weak neutral current 'charge' and 'magnetic' form factors, G_E^Z and G_M^Z, respectively. These can be extracted from a set of parity violating electron-proton scattering measurements. If one assumes a relationship between the proton and neutron structure in that the proton and neutron differ only by the interchange of "up" and "down" quarks, i.e., isospin symmetry, the strange quark (as well as the up and down quark) contribution to the charge and magnetic form factors of the nucleon can be determined. This would result from taking appropriate linear combinations of the weak neutral form factors and their electromagnetic counterparts.

Determinations of both the charge and magnetic strange quark form factors are of fundamental interest, as they would constitute the first direct evidence of the quark sea in low energy observables. The objective of the $G0$ experiment is to determine these contributions to the proton form factors at the few percent level. Observations at high energy suggest that the strange quarks carry about 1/2 as much momentum as up and down quarks in the sea. It is important to determine both the role of the quark sea and the relevance of strange quarks at low energy where there

are voids in understanding the theory of the strong interaction, quantum chromodynamics (QCD). Even if the strange quark contributions do not amount to the level of sensitivity of the experiment, upper limit determinations at this level are as valuable as non-zero results. The matrix elements, G_E^Z and G_M^Z, are also relevant to the discussions of the Ellis-Jaffe sum rule and of the pion-nucleon sigma term; there is evidence in both of these that the strange quark contribution is larger than expected. The $G0$ experiment will allow the determination of the strange quark contributions to the proton charge and magnetic form factors in a much more straightforward manner than is possible with regard to the corresponding observables in the above two determinations.

In the $G0$ experiment parity violating longitudinal analyzing powers will be measured in electron-proton scattering in the range $0.1 \leq Q^2 \leq 1.0$ GeV^2 at both forward and backward angles. The longitudinal analyzing power is defined as

$$A_z = \frac{1}{P}\,[\sigma^+(\theta) - \sigma^-(\theta)]/[\sigma^+(\theta) + \sigma^-(\theta)]\ ,$$

with P the polarization of the incident electron beam and the $+$ and $-$ signs indicating the helicity state. Making pairs of measurements at forward and backward angles will allow the separation of G_E^Z and G_M^Z. Predicted longitudinal analyzing powers range from about (–3 to 35) $\times 10^{-6}$; it is planned to measure the longitudinal analyzing powers with statistical uncertainties of $\Delta A/A = 5\%$ and systematic uncertainties related to helicity correlated effects of $\Delta A/A \leq 2.5 \times 10^{-7}$. In the first phase of the experiment longitudinal analyzing powers will be measured concurrently at seven values of the momentum transfer in the range $0.1 \leq Q^2 \leq 1.0$ GeV^2. With an electron beam polarization of 0.49, the time required to reach this precision in the first phase measurement will be about 700 hours. It appears highly probable that by the time of data-taking for the $G0$ experiment higher beam polarizations will have been reached, reducing the data-taking time by close to a factor of two. However, it must be realized that it is not the actual data-taking time that governs the length of the experiment but rather making elaborate control measurements to determine the corrections that have to be made to the measured asymmetries and to understand systematic errors. Using the result for G_M^Z at $Q^2 = 0.1\ GeV^2$ from the SAMPLE experiment now being performed at the MIT-Bates Laboratory, it would be possible to separate the charge and magnetic form factors at the lowest Q^2 bin after the first phase measurement. In the second phase experiment each subsequent backward angle analyzing power measurement would require from 0.5 to 1 month of running time. It should be noted that the overall uncertainties quoted for the recent parity violation experiments at PSI and the Univ. of Bonn and quoted for the systematic uncertainties in the parity violation experiments at MIT-Bates and Mainz of a few times 10^{-8} suggest that systematic uncertainties of a few times 10^{-7} should be attainable in the $G0$ experiment.

Canadian contribution to the *G*0 experiment

The $G0$ experiment will be executed by a collaboration of scientists from the Univ. of Illinois at Urbana-Champaign, California Institute of Technology/ Univ. of Maryland, Carnegie-Mellon Univ., TJNAF, Norfolk State Univ., and the Canadian subgroup from the universities of Manitoba, Northern British Columbia, Regina, and from TRIUMF. The Canadian subgroup has been asked to : (i) develop and provide specialized photomultiplier tube bases for the main detector arrays; (ii) provide specific lightguide sections of the main detector array; (iii) design and test specialized beam monitors and control apparatus; (iv) provide specialized "parity-type" electronics to read out beam current, position, and energy monitors; and (v) design, build and test an automated magnetic field measuring apparatus complete with its own data acquisition system. With the exception of the Canadian contribution, the funding for the $G0$ experiment will be borne by the US Department of Energy through TJNAF and the US National Science Foundation.

Over the past year, much progress has been made pursuing designs for the various components listed above.

The *G*0 main detector array

The heart of the $G0$ detection system is a spectrometer which consists of an 8 sector toroidal magnet, with an array of scintillation detectors located at the focal surface of each sector. Due to geometry, resolution, and rates considerations, the shapes of both the prototype scintillators and their associated lightguides have become quite elaborate. Since data will not be acquired in event-by-event mode in this experiment, and since the scintillator arrays are the only detectors to measure the scattered particles, the performance of these focal surface detectors are of critical importance. The timing and pulse shape characteristics of this system must be fine-tuned at the hardware level because it will not be possible to reconstruct individual events. As such, special demands are made on the photomultiplier tubes and especially on their associated divider/base circuit. Much progress has been made on the design of the bases, resulting in 4 prototype bases being constructed and delivered to TJNAF for further tests. The prototype bases were constructed at TRIUMF and represent a sophisticated design (both electronically and

mechanically) which has been refined over many iterations.

An integral part of the prototype bases are specialized lightguide couplers which enhance the mechanical stability of the detector-PMT interface. These and possibly other specialized lightguide sections of the main detector array will be the responsibility of the Canadian subgroup and will be produced at TRIUMF when the design of the prototype detectors is completed. Due to the resident expertise at TRIUMF in producing high quality scintillation detectors and lightguides, the Canadian subgroup has also been asked to help in the production of the prototype detectors. Several 'rough cut' prototype scintillators were sent to TRIUMF this summer, where they were finished and then delivered to TJNAF to undergo further bench tests.

Resonant cavity position and current monitors

Five sets of XYQ monitors will be required in order to measure the beam current (charge) and trajectory (positions and angles) at several critical locations (directly upstream of the target, at an upstream dispersed focus, and further upstream in the beam line). The proposed current monitor will be of the resonant cavity type. Presently, the design consists of a cylindrical cavity operating in the TM010 mode at 1497 MHz. A beam current sensitivity of $\pm 4 \times 10^{-5}$ measured in a 33 ms integration time will be required to monitor and correct for possible helicity correlated intensity modulations. For the beam position monitors (BPM), there are two designs under consideration. The presently existing BPM's consist of stripline monitors operating in a special switched electrode electronics (SEE) mode. An alternate proposal involves the use of resonant cavities, likely a pair of cylindrical cavities (X and Y) operating in the TM110 mode. In either case, a spatial resolution of better than 25 μm at an integration time of 33 ms will be required.

The beam current and the stripline position monitors were used in tests during a recent engineering run in July at TJNAF, and will be discussed below.

Specialized parity electronics

To read out the analog signals from the various beam current and position monitors, specialized parity-type electronics will be required. Much of this electronics, such as precision analog subtractors/dividers and precision voltage-to-frequency converters, has already been designed and used by members of the Canadian subgroup in their parity experiments at TRIUMF. Recent modifications, driven by the requirements of the $G0$ experiment, were made to some of these electronics modules and they were operated successfully at the July engineering run at TJNAF.

July test beam/engineering run

Test beam time was made available for a $G0$ engineering run in Hall C at TJNAF in July. The run was organized by members of the $G0$ Canadian subgroup and personnel from TJNAF (Hall C), with much of the readout electronics provided by the Canadian subgroup. The parity precision subtractors/dividers and V-f converters were readily adapted to the TJNAF beam monitors and operated in a trouble-free manner, and the suitability of the equipment, techniques and expertise developed through the parity experiment at TRIUMF was amply demonstrated.

Helicity correlated properties of the TJNAF polarized electron beam and the noise characteristics of some of the beam monitors were successfully measured. Figure 22 shows some sample data for the helicity correlated position modulations ($\Delta X, \Delta Y$) at 3 sets of monitors (BPMC07, BPMC12, and BPMH00) located downstream of the TJNAF beam switchyard (C07), in an energy-dispersed location in the C-line arc section (C12), and in the Hall C experimental area (H00), respectively. Also shown at the bottom of Fig. 22 are sample data for the helicity correlated beam intensity modulations ($\Delta I/I$) at 2 current monitors BCM1 and BCM2 located in the Hall C experimental area. Preliminary on-line results indicate that the beam current monitors will likely meet the specification requirements of $\Delta Q/Q \leq 4 \times 10^{-5}$. The stripline SEE monitors were able to provide position determinations with $\Delta X \leq 200 - 400$ nm over the course of a 10 minute run, which may be close to the specification requirements. However, a more detailed analysis is required and is currently under way. Further test beam time is also planned for the coming year.

Canadian subgroup of the $G0$ collaboration: J. Birchall, W.R. Falk, L. Lee, S.A. Page, W.D. Ramsay, W.T.H. van Oers, R.J. Woo (Manitoba); E. Korkmaz, G. O'Reilly (Northern British Columbia); C.A. Davis (TRIUMF).

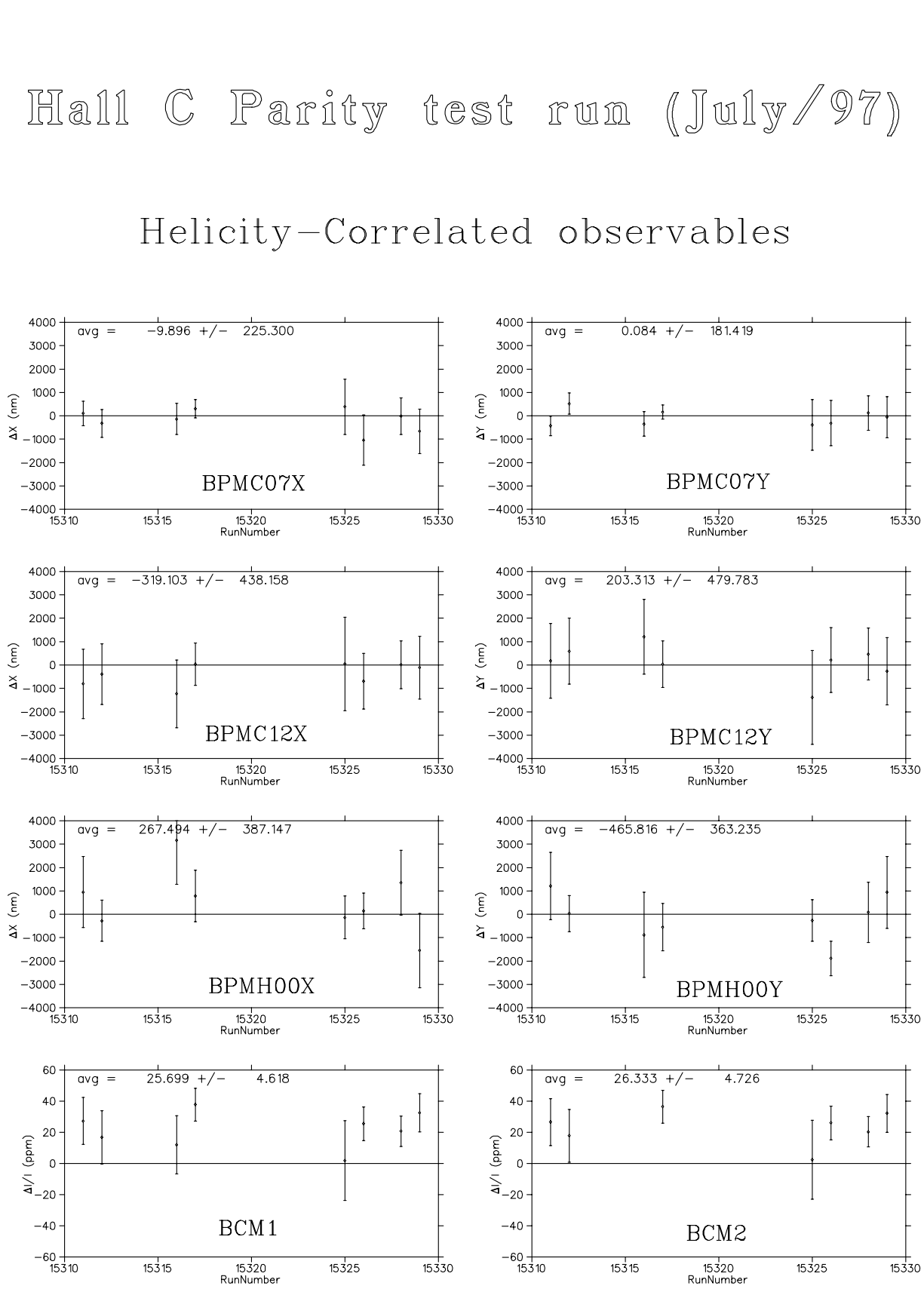

Fig. 22. Sample data from July engineering run. Helicity-correlated modulations in beam positions (at an upstream location (C07), an upstream energy-dispersed location (C12), and in the experimental hall (H00)) and beam current. Each data point represents a short run lasting between 10–15 minutes. Note that the helicity-correlated intensity modulation of about 25×10^{-6} is sufficiently small that it should not be a problem for the $G0$ measurement.